Session 7

Turbine Systems

7.1 Development of Topping Combustor for Advanced Concept Pressurized Fluidized Bed Combustion

CONTRACT INFORMATION

Contract Number	DE-AC21-86MC21023
Contractor	Westinghouse Electric Corporation 4400 Alafaya Trail Orlando, Florida 32826-2399 (407) 281-2000
Contract Project Manager	William F. Domeracki
Principal Investigators	Thomas E. Dowdy Dennis Bachovchin
METC Project Manager	Donald L. Bonk
Period of Performance	June 1, 1988 to December 31, 1994 (Phase II)
Schedule and Milestones	

FY94 Program Schedule

OBJECTIVES

The objective of this program is to develop a topping combustor to operate in a Second-Generation Pressurized Fluidized Bed (PFBC) Combined Cycle power generation system. The combustor must be able to:

- Lightoff with a high heating value fuel and compressor discharge air to heat the fluidized bed(s) and provide power for PFBC and carbonizer off-line.
- Operate with 1600°F (870°C) oxygen depleted air from the PFBC and high heating value fuel to handle carbonizer off-line conditions.
- Ramp up to 100% carbonizer syngas firing (normal operation) by firing a blend of decreasing high heating value fuel and increasing low heating value syngas.
- Utilize the vitiated air, at temperatures up to 1600°F (870°C) for as much cooling of the metal combustor as possible, thus minimizing

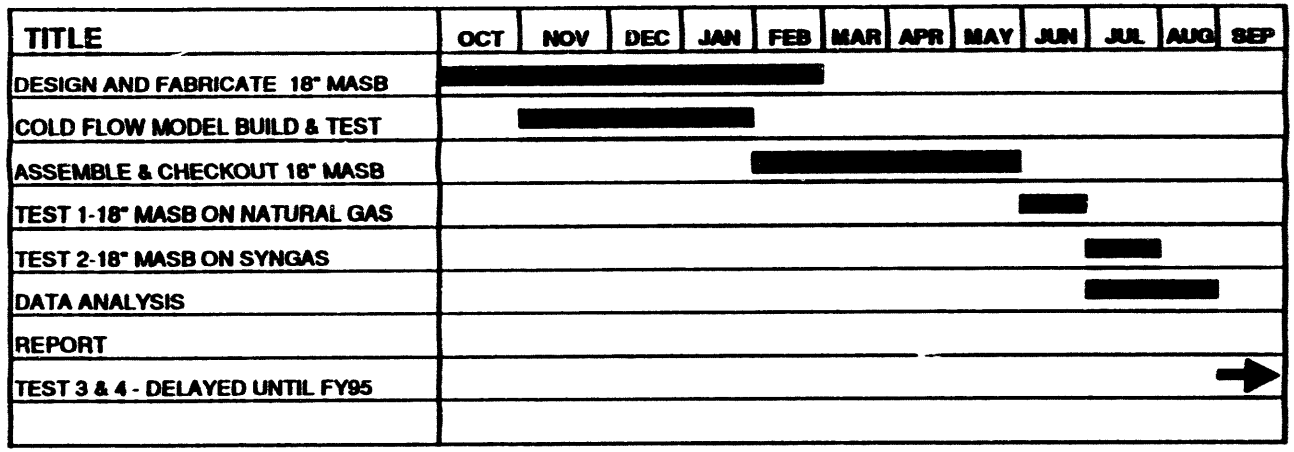

FY94 Program Schedule

the compressor bypass air needed for combustor cooling.

- Provide an acceptable exit temperature pattern at the desired burner outlet temperature (BOT).

- Minimize the conversion of fuel bound nitrogen (FBN) present in the syngas to NO_x.

- Have acceptably high combustion efficiency, and low emissions of carbon monoxide, UHC, etc.

BACKGROUND INFORMATION

A project team consisting of Foster Wheeler Development Corporation, Westinghouse Electric Corporation, Gilbert/Commonwealth, and the Institute of Gas Technology, are developing a Second Generation Pressurized Fluidized Bed System. Foster Wheeler is developing a carbonizer (a partial gasifier) and a pressurized fluidized bed combustor. Both of these units operate at a nominal 1600°F (870°C) for optimal sulfur retention.

Since this temperature is well below the current combustion turbine burner outlet temperature (BOT) operation of 2350°F (1290° C), to reach commercialization, a topping combustor and hot gas cleanup (HGCU) equipment must be developed. Westinghouse is participating in the development of the HGCU equipment (reported elsewhere at this conference) and the topping combustor. Work performed on the topping combustor since the last contractor's review meeting (Domeracki, et al. 1993) is presented in this paper.

This paper updates only one part of a multi-phase program. This test program is part of Phase II of a three-phase ongoing DOE/METC program. Phase I involved the conceptual and economic study (Robertson et al., 1988); Phase II addresses subscale testing of components; Phase III will cover pilot plant testing of components integrated into one combustion system.

PROJECT DESCRIPTION

The topping combustor in this cycle must utilize a low heating value syngas produced from the carbonizer at approximately 1600°F (870°C) and 150 to 210 psi (1.0 to 1.4 MPa).

The syngas entering the topping combustor has been previously cleaned of particulates and alkali by the HGCU equipment. In addition to the combustible materials (primarily CO, H_2 and CH_4) it also contains significant fuel bound nitrogen (FBN) from the coal present as ammonia (NH_3) and other compounds. This FBN is significant because it will selectively convert to NO_x in the highly oxidizing conditions of standard combustion turbine combustors.

The hot syngas must be burned with the vitiated (partially burned) air from the pressurized fluidized bed combustor (PFBC). This air is at 1600°F (870°C) and still contains sufficient oxygen for combustion and has been cleaned of particulates and alkali in a separate HGCU system. To obtain optimum efficiency, the 1600°F air must also be utilized to cool the metal combustor surfaces to as great an extent as possible, though a small amount of compressor discharge air at a lower temperature, 700°F (370°C) will also be needed for combustor rich zone cooling.

These application requirements indicate that a specially designed rich-quench-lean (RQL) combustor be used and Westinghouse has selected the Multi-Annular Swirl Burner (MASB, Beér, 1965& to 1969&) for further development for this application.

In selecting a combustor design that will withstand the conditions expected in the topping application, the effective utilization of the 1600°F (870°C) air could satisfy the wall cooling challenge by maintaining a cooling air layer of substantial thickness. Thick layers of cooling air at the leading edge of each inlet section are easily achieved if the combustor is made up of concentric annular passages. In addition to wall cooling considerations, the burner must inhibit the formation of NO_x from syngas that contains FBN, have high combustion efficiency, produce an acceptable exhaust temperature pattern, exhibit good stability, and be able to light off at cold plant conditions. The MASB has demonstrated that it can meet all of these requirements.

This paper reports the results of tests of a 14" diameter topping combustor with a modified fuel-rich zone conducted in June 1993, design of an 18" diameter topping combustor to be tested in June 1994 and afterwards, and results of a 50% scale cold flow model which has been built and tested.

RESULTS

June 1993 14" Diameter Test Results

In June 1993 a test was performed at the University of Tennessee Space Institute (UTSI) with a modified 14" diameter MASB. This test was considered to be very successful, as will be shown in the following data and text.

The "old" MASB, which had been utilized in pre-1993 tests (Figure 1) was modified, as shown in Figure 2. This design was described in the 1993 contractors review, (Domeracki, 1993). Essentially the new design increased the residence time in the fuel-rich zone, obtained backmixing and a controlled reaction temperature in the fuel rich zone, and tested the most recent "Wilsonville" paste feed composition. If sufficient fuel remained (which it did) we were to also test the "Wilsonville" dry feed compositions. These compositions, as predicted and as tested, are shown in Tables 1 & 2.

Table 1. Wilsonville Paste Syngas Composition

	Volume Predicted	Percent as Tested
CO	14.31	14.31
H_2O	11.44	11.44
CO_2	9.44	0
H_2	15.48	15.48
CH_4	2.15	2.15
N_2	46.45	56.45
NH_3	.17	.17

Table 2. Wilsonville Dry Syngas Composition

	Volume Predicted	Percent as Tested
CO	17.22	17.22
H_2O	9.17	9.17
CO_2	7.82	0
H_2	18.01	18.01
CH_4	2.62	2.62
N_2	44.42	52.76
NH_3	.23	.23

The main interest was to confirm the predicted NH_3 to NO_x conversion. The new 14" nozzle (Figure 2) was designed to improve recirculation and to have the rich zone operate within a temperature range of 2900°F +/- 100°F. Due to higher than anticipated leakage around the MASB (i.e., lower than measured oxidizer flow through the MASB), most calculated (allowing for

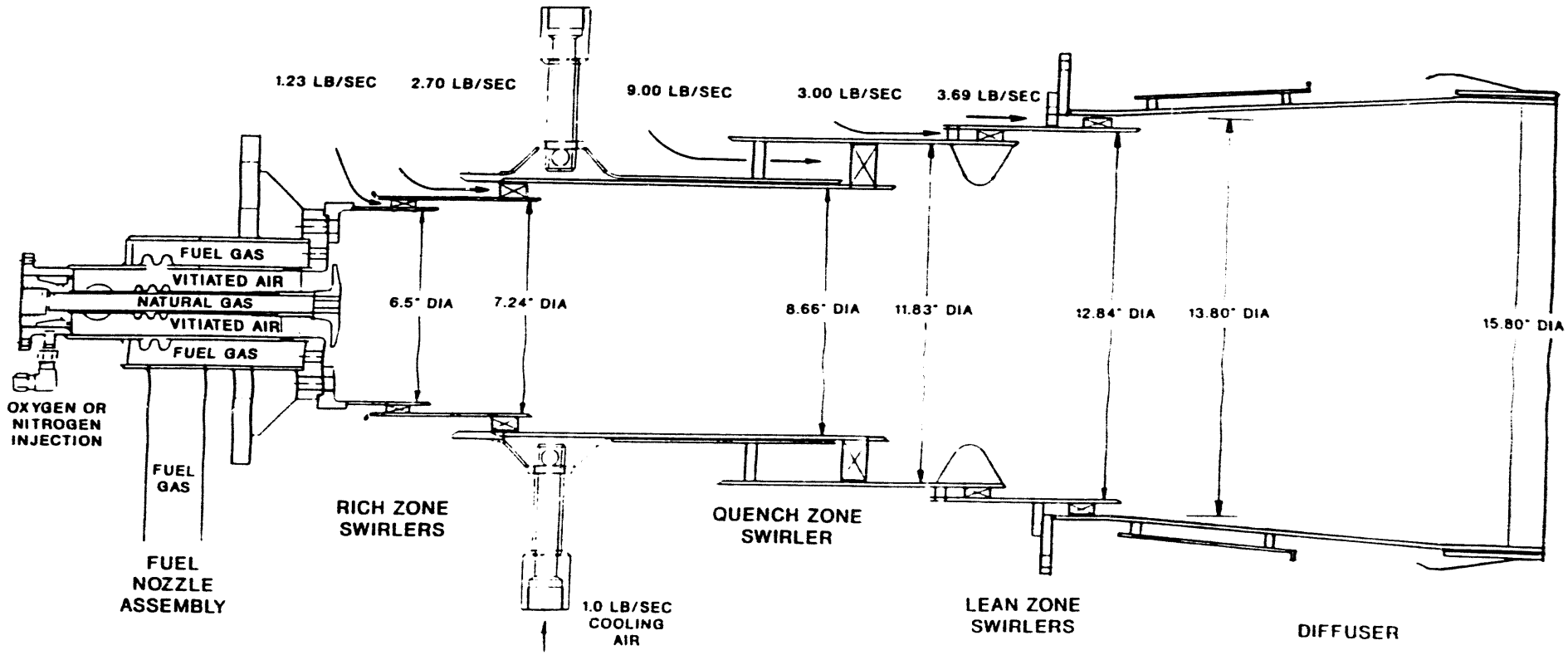

Figure 1. Old 14" MASB Design

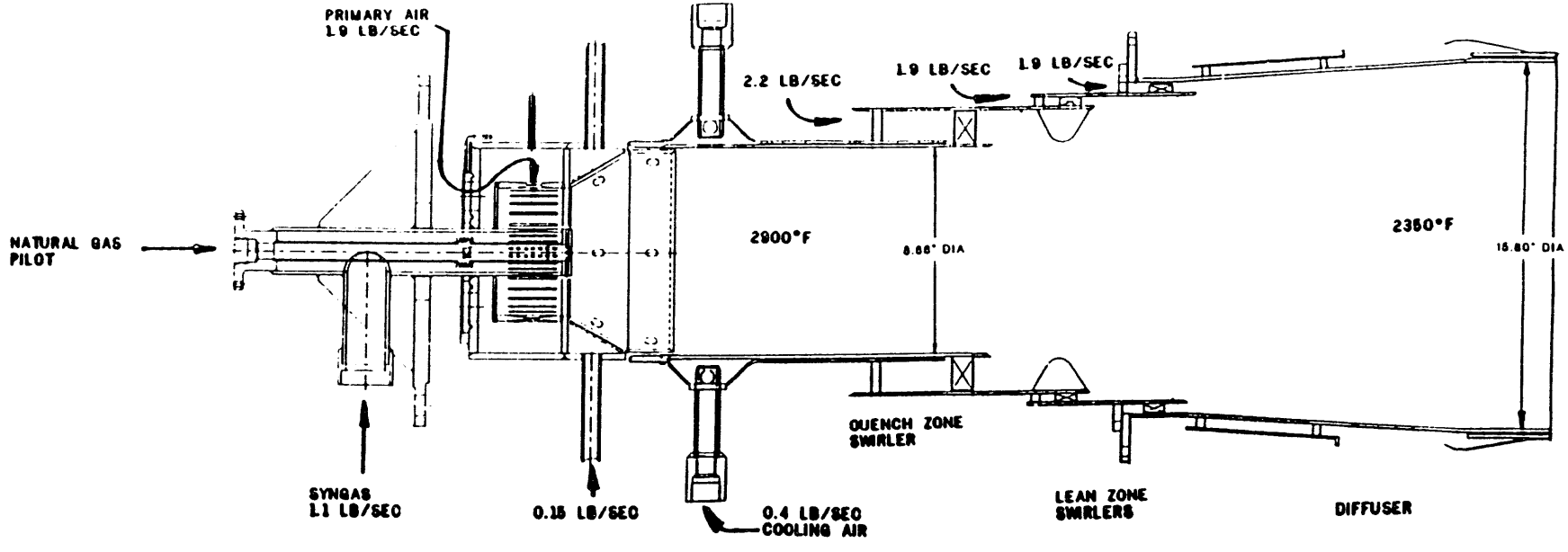

Figure 2. New 14" MASB Design

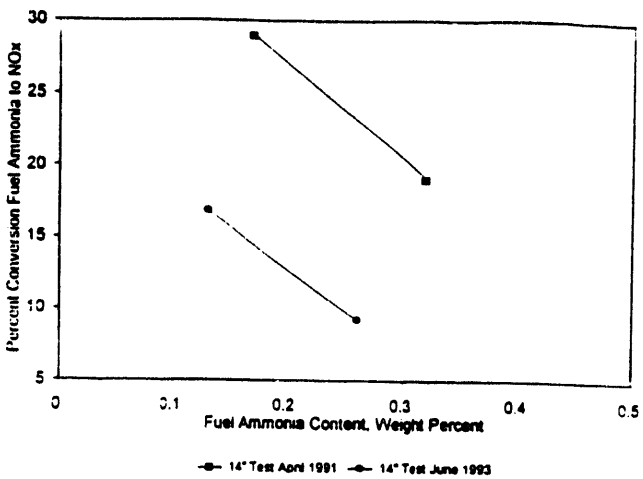

Figure 3. Comparison of 1991 and 1993 14" MASB Ammonia Conversion

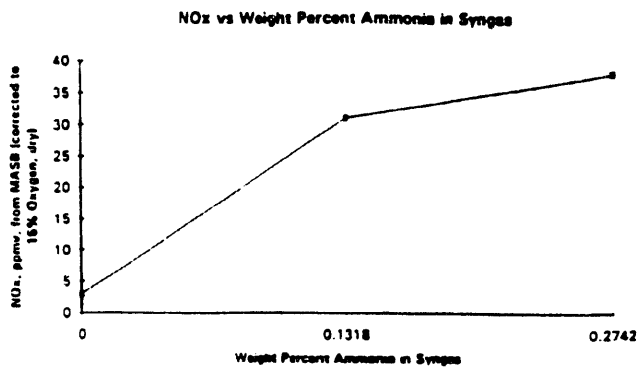

Figure 4. NOx vs Weight Percent Ammonia in Syngas

leakage) rich zone temperatures were between 3000°F and 3300°F. Thus, in spite of running at this off design condition, the bulk of the NH_3 conversions to NO_X were about 10 to 20 percent (Figure 3). Figure 3 shows that this was significantly better than previous test results at similar conditions. This was within our target range of expected results and thus demonstrated that our objective of demonstrating that our methodology for the redesign of the rich zone was acceptable and on the conservative side.

Carbon monoxide emissions were near zero at all points of the test with syngas firing. Even though the oil-fired direct heated preheater generated some carbonmonoxide, it was usually below detection limits of the gas analyzers at the MASB exit.

Modifications for 14" Test

A fuel blending station was added at UTSI, so that the cost of syngas (which had been bought premixed) could be lowered, the run time extended, and any desired composition of syngas could be produced by on-line adjustment. Prior computational fluid dynamics (CFD) and chemical kinetic computations had indicated that the previously utilized syngas entrance temperature of 800°F (425°C) at UTSI was not sufficiently high to rapidly initiate the desired reactions (Domeracki, 1993). Therefore, the syngas heater at UTSI was modified to provide 1200°F (650°C) syngas to the MASB.

Most of the results presented in this section represent percent conversion of ammonia to NO_X. However, Figure 4 shows three data points taken over a few minutes of time. All conditions were held constant except for the weight percent ammonia in the syngas. Two things should be noted from this plot:

First, with no ammonia in the syngas, very little NO_X was formed. The 3ppm plotted cannot be assumed to be an absolute value, since the preheater was generating approximately one order

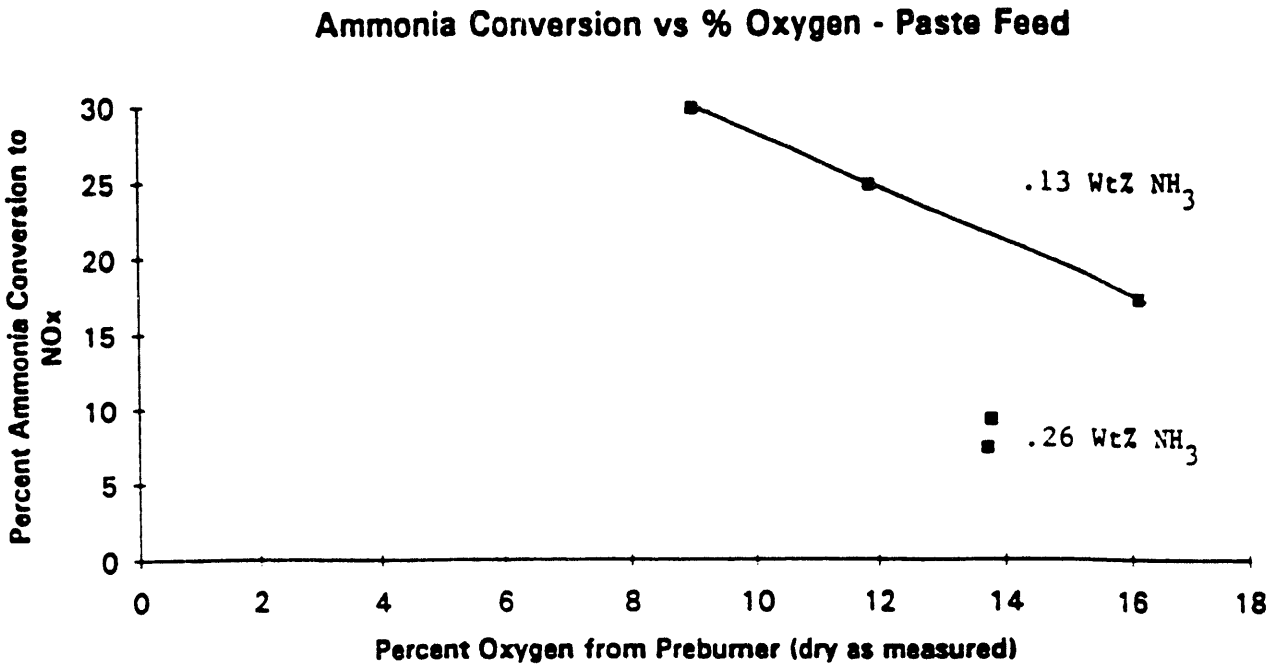

Figure 5. Ammonia Conversion vs % Oxygen - Paste Feed

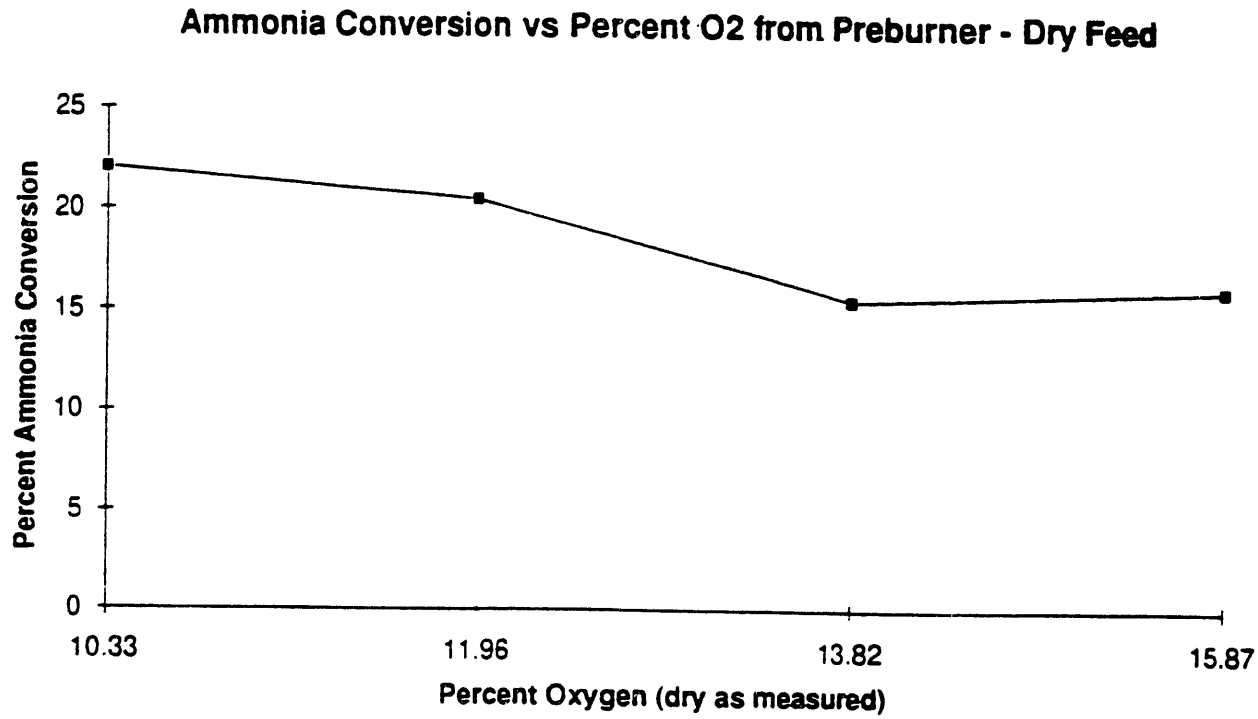

Figure 6. Ammonia Conversion vs % Oxygen - Dry Feed

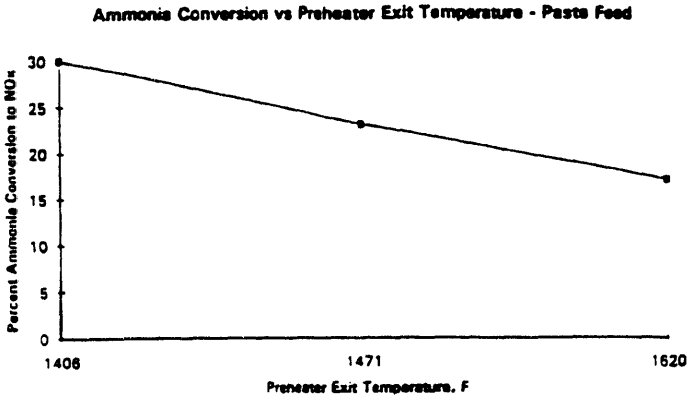

Figure 7. Ammonia Conversion vs Preheat Temperature - Dry Feed

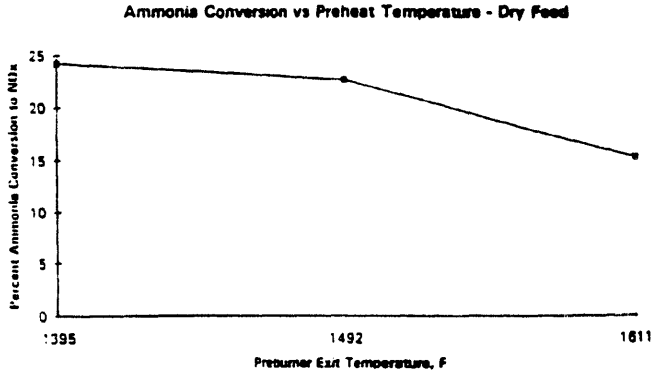

Figure 8. Ammonia Conversion vs Preheat Temperature - Dry Feed

of magnitude more NO_X, and this value is calculated by difference between two much larger numbers, (i.e. NO_X - NO_X in). Still, the combined thermal and prompt NO_X formed is extremely low.

Second, between 0.13 weight percent NH_3 and 0.27 weight percent, the slope is relatively flat. Thus the absolute NO_X emissions from the MASB is relatively insensitive to ammonia content, as our analysis predicts.

Figures 5 and 6 show that the percent ammonia conversion is an inverse function of oxygen content from the preburner. Figures 7 and 8 show that the percent ammonia conversion decreases with increasing preburner exit temperature. Both of these can be explained by the higher inlet oxygen or higher inlet vitiated air temperature which will initiate the NH_3 to N_2 conversion in a shorter period of time. With corrections made for higher than expected leakage of the oxidizer, corresponding with higher than expected rich zone temperature, the calculated flame temperature in the rich zone was higher than desired in most tests. However, even with the hotter than desired temperatures, the NH_3 conversion was equal to or below our design predictions. Thus we conclude that our design simulation technique is acceptable, though conservative.

Cold Flow Model Pattern Verification

A half scale cold flow model with similar Reynolds number and velocity profiles as the hot 18 inch MASB at full pressure was tested to verify the flow characteristics required and expected. Table 3 compares the hot 18 inch and the cold model MASBs.

Extensive mapping of the flow pattern in the MASB was performed using a two-dimensional flow probe (United Sensor model W-187), which measures yaw angle, static pressure, and dynamic pressure, giving the direction (in the tangential/axial plane) and magnitude of flow velocity as a function of axial and radial positions.

Figure 9 is a map of the resulting axial velocities. The results verified CFD modeling projections and the existence of desired flow patterns. The following significant features are apparent:

1. A strong donut-shaped recirculation region was confirmed in the wake of the bluff body end of the fuel swirler. This extends about one third of the way down the rich zone cylinder. The existence of this recirculation is essential for backmixing of free radicals to initiate combustion early so the whole rich zone residence time is available for the relatively slow conversion of NH_3 to N_2.

2. There is an absolute boundary (location C to C_2) between the rich and quench zones through which no reverse flow occurs, thereby guaranteeing the existence of fuel rich combustion.

3. Swirl was very strong (100 to 200 ft/sec tangential velocity), for good stabilization.

4. Axial velocities are also high near the wall for necessary effective wall cooling.

Design of the 18-Inch MASB

The 18-inch MASB (Figure 10) is intended to be a full-scale prototype of a single basket, incorporating all commercially required features. Therefore, the 18-inch MASB has been designed to accomplish the following four major technology advancements with respect to the 14 inch MASB.

1. Scale up from half-scale (in terms of mass flow) to full-scale.

   The 18-inch MASB is the same scale as planned for the Wilsonville Pilot Facility. Future applications to commercial combustion turbines would feature a multiple number of cans of this design. Table 4 shows the typical achieved conditions in the 14 inch MASB test, the planned operating conditions for the 18-inch MASB, and the conditions expected for the Wilsonville MASB.

   The rich zone diameter for the 14-inch MASB was 8.5 inches, whereas for the 18-inch MASB, this diameter is 14 inches. All fuel nozzle end dimensions are a direct geometric scale up.

2. Optimize combustor rich zone performance for better conversion of NH_3 to N_2.

   Although very good NO_x performance was achieved in the 14-inch testing, analysis indicates that better performance is possible. Table 5 shows the effects of rich zone equivalence ratio and residence time on NO_x generation in the MASB. The first line represents 14-inch achieved performance. These calculations were made using a Westinghouse combustion chemical kinetic data base with the Sandia Chemkin-II chemical kinetics modeling program.

   Table 5 shows that if the rich zone stoichiometry is too lean substantial NO_x is generated in the rich zone itself. If too rich, then NH_3 survives the rich zone to be converted to NO_x in the downstream lean regions. An optimum occurs in the 1.4 to 1.5 equivalence ratio range, as shown in Table 5. Also, performance is better with increased residence time.

   Consequently, an increase in residence time to 40 msec from 25 msec, by increasing length, and an increase in fuel equivalence ratio to 1.4 from 1.2 are goals of the 18-inch design and test plan.

18 Inch MASB Design
Cold Model Results

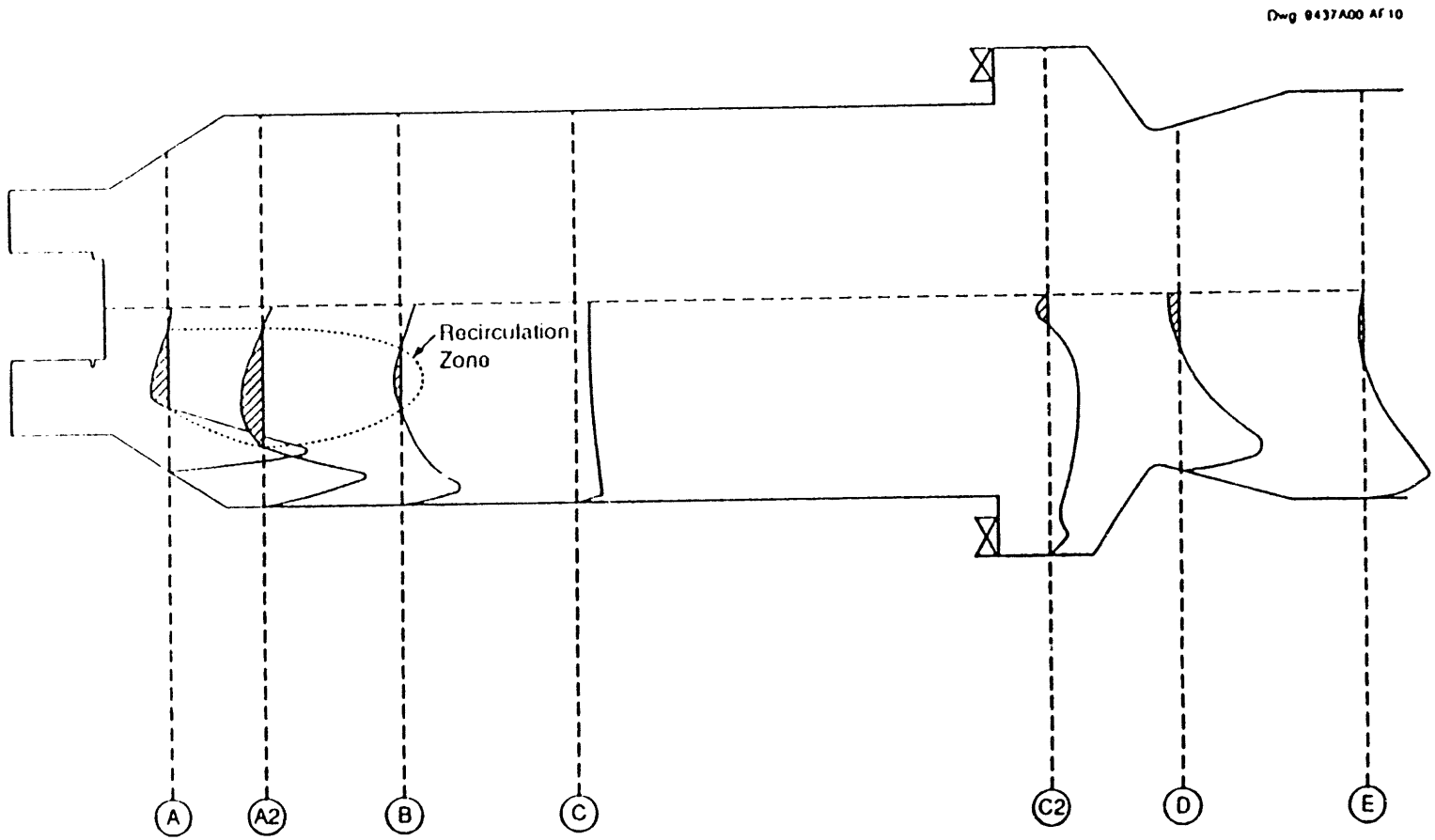

Figure 9. 18 Inch MASB Design Cold Model Results

Table 3. Similarity of Hot 18-Inch MASB and Cold Model

	18-Inch Hot MASB	Cold Model
Rich zone:		
Diameter, in.	14.5	7.0
Length, in.	27.9	13.5
Temperature, F	2900	70
Pressure, psia	160	16.2
Gas density, lbm/ft3	0.124	0.082
Gas velocity, ft/sec	55	52
Gas viscosity, lbm/ft-sec	0.00004	0.000012
Reynolds No.	206,000	206,000
Quench zone:		
Diameter, in.	12.0	5.8
Length, in.	6.9	3.6
Temperature, F	2850	70
Pressure, atm	160	16.2
Gas density, lbm/ft3	0.126	0.082
Gas velocity, ft/sec	120	114
Gas viscosity, lbm/ft-sec	0.00004	0.000012
Reynolds No.	380,000	380,000

3. Incorporate and demonstrate natural gas firing capability in both vitiated air and compressor air.

   The design features the capability for natural gas firing via a central dual fuel burner as shown in Figure 10 and magnified in Figure 11. A modified Pabst burner is utilized for natural gas combustion. Design natural gas consumption rates are 0.2 lb/sec for vitiated air firing and 0.4 lb/sec for compressor air firing. When doing so, steam (1 lb per lb natural gas) is injected through the syngas swirlers, both to keep it purged and to moderate rich zone temperature. Since this is a rich/lean combustor, the steam is not needed for NO_x reduction. A specially designed axial ignitor rod is used. These technologies are now to be demonstrated.

4. Incorporate improved mechanical designs.

   A number of hardware mechanical improvements have been incorporated.

   - The convergent-divergent flow deflector in the quench zone (see Figure 2) is now directly cooled by the incoming dilution section vitiated air in contract to the uncooled 14 inch flow vitiated air, in contrast to the uncooled 14-inch deflector where some thermal distress occurred. Also, a thermal barrier coating is now applied to all internal surfaces.

18 Inch MASB Design

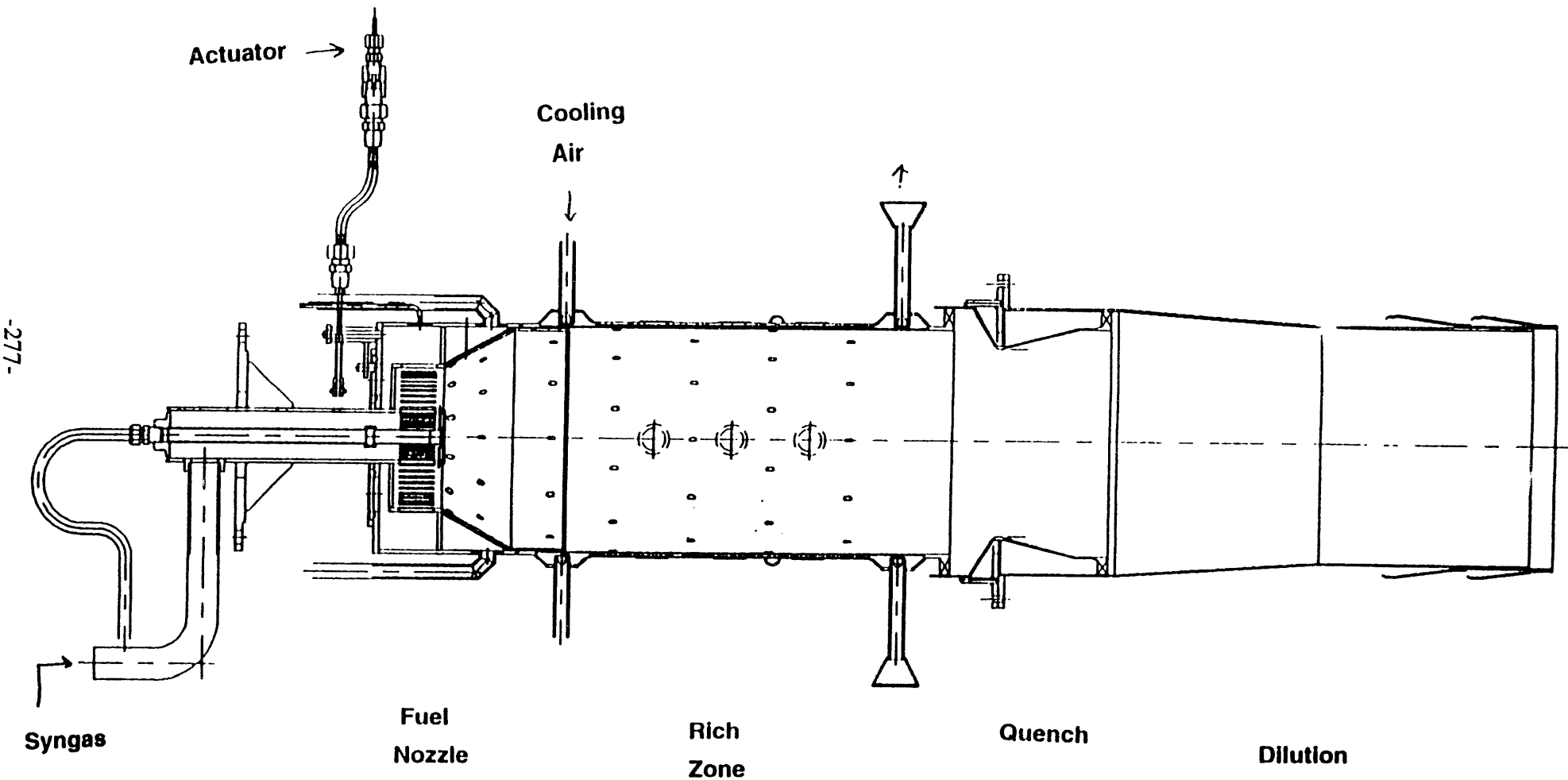

Figure 10. 18 Inch MASB Design

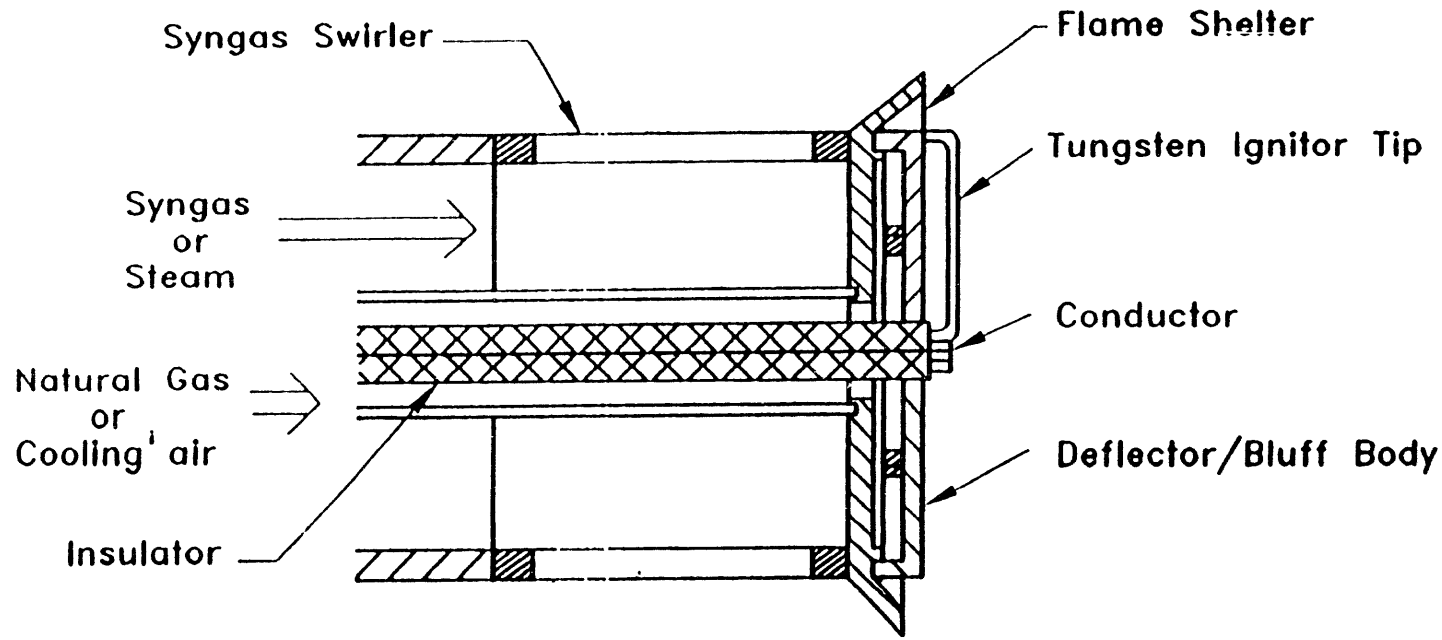
Syngas Swirler
Flame Shelter
Tungsten Ignitor Tip
Syngas
or
Steam
Conductor
Natural Gas
or
Cooling air
Deflector/Bluff Body
Insulator

Figure 11.

Table 4. Scale up of the MASB

	UTSI 14"	UTSI 18"	Wilsonville 18"
Syngas			
Temperature, xF	1200	1200	1600
Vitiated air			
Temperature, xF	1600	1600	1470
Pressure, atm (abs)	10	7.3	10
Rich zone velocity, ft/sec	45	55	55
Rich zone res. time, msec	28	45	43
Pressure drop, psid	2.8	2.8	2.5
Temperatures, xF			
Rich zone	3100	2750	2800
Quench zone	2650	2850	2850
Exit	2250	2350	2100
Turbine inlet			1977
Flows, lb/sec			
Syngas	0.7	2.6	3.3
Primary vit. air	0.9	2.0	4.3
Quench vit. air	0.4	3.2	6.8
Dilution vit. air	2.2	6.4	9.0
Cooling air	0.9	0.8	5.0

Table 5. Theoretical Fuel NO_x Formation vs. Rich Zone Parameters

Case	Equivalence ratio	Res. time,	NH_3 from rich zone, ppmv	NO_x from rich zone, ppmv	Fuel NO_x from MASB, ppmv
1	1.2	25	15	150	36
1	1.2	45	14	132	32
2	1.5	25	61	17	18
2	1.5	45	33	14	12
3	1.7	25	317	12	57
3	1.7	45	199	12	38
4	2.0	25	725	10	109
4	2.0	45	514	10	78

7.2 Development and Testing of Low Btu Fuel Gas Turbine Combustors

CONTRACT INFORMATION

Contract Number DE-AC21-87MC23170

Contractor
GE Environmental Services, Inc.
200 N. Seventh St.
Lebanon, PA. 17042
(717) 274-7000

Contractor Project Manager Stephen Bevan

Principal Investigators
Nesim Abuaf, GE Corporate Research and Development
Alan S. Feitelberg
Stephen L. Hung
Martin S. Samuels
Anil K. Tolpadi

METC Project Manager Justin L. Beeson

Period of Performance September 30, 1987 to September 30, 1994

Schedule and Milestones

Program Schedule

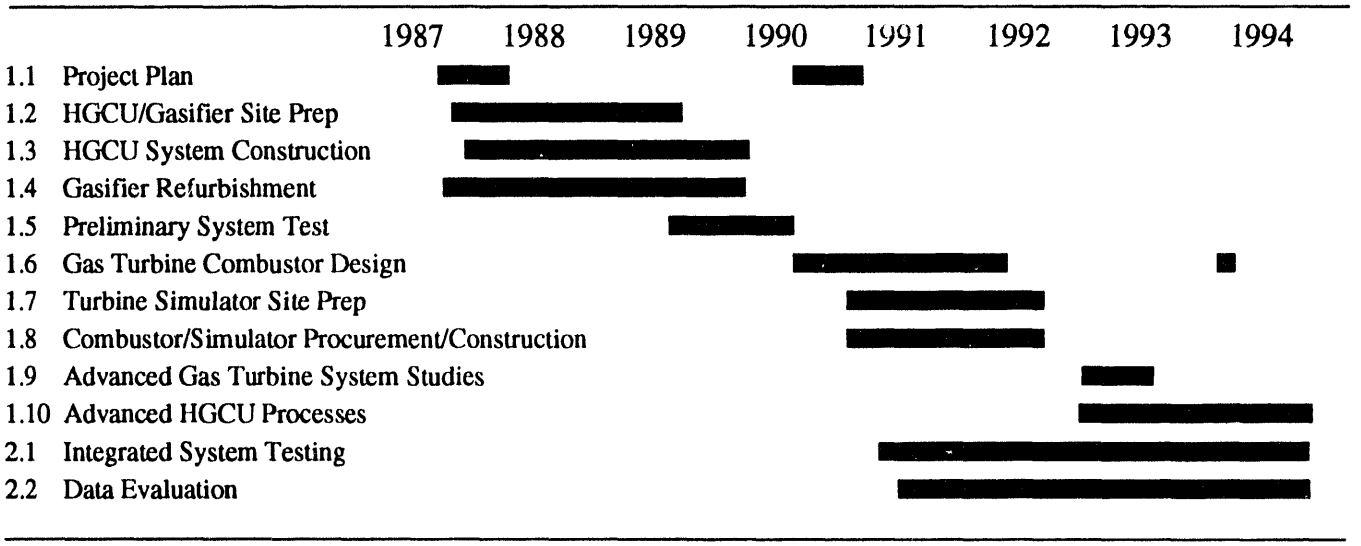

OBJECTIVES

The integrated gasification combined cycle (IGCC) concept represents a highly efficient and environmentally compatible advanced coal fueled power generation technology. When IGCC is coupled with high temperature desulfurization, or hot gas cleanup (HGCU), the efficiency and cost advantage of IGCC is further improved with respect to systems based on conventional low temperature gas cleanup.

Commercialization of the IGCC/HGCU concept requires successful development of combustion systems for high temperature low Btu fuel in gas turbines. Toward this goal, a turbine combustion system simulator has been designed, constructed, and fired with high temperature low Btu fuel. Fuel is supplied by a pilot scale fixed bed gasifier and hot gas desulfurization system. The primary objectives of this project are: (1) demonstration of long term operability of the turbine simulator with high temperature low Btu fuel; (2) characterization of particulates and other contaminants in the fuel as well as deposits in the fuel nozzle, combustor, and first stage nozzle; and (3) measurement of NO_x, CO, unburned hydrocarbons, trace element, and particulate emissions.

In a related project, a reduced scale rich-quench-lean (RQL) gas turbine combustor has been designed, constructed, and fired with simulated low Btu fuel. The overall objective of this work is to develop an RQL combustor with lower conversion of fuel bound nitrogen (FBN) to NO_x than a conventional combustor.

BACKGROUND INFORMATION

Combustion of the high temperature (~1000°F) low Btu fuel produced from an IGCC/HGCU system is significantly different from the combustion of typical gas turbine fuels, such as natural gas and fuel oils. Differences in the air/fuel ratio, fuel composition, and fuel temperature affect many of the combustor operating parameters including the lean blowout limit, flame stability, and emissions. These differences require modification of the fuel nozzle and combustor liner. In addition, gas turbines used in IGCC/HGCU applications will require fuel control valves that are capable of operating with high temperature low Btu fuel. Other concerns include the possibility that particles and vapor phase contaminants in the fuel may form deposits on and/or cause the corrosion of the fuel nozzle, combustor liner, and turbine blades.

PROJECT DESCRIPTION

Turbine Simulator

Figure 1 shows the low Btu gas turbine simulator that has been constructed and integrated with the coal gasification/hot gas cleanup facility at GE Corporate Research and Development in Schenectady NY. The pilot scale gasification/hot gas cleanup system consists of a fixed bed gasifier, a sodium bicarbonate based halogen removal system, a moving bed high temperature desulfurization system, and a polishing cyclone. The turbine simulator is designed to operate at the full capacity of the gasifier, 8000 lb./hr of fuel gas from the gasification of 1800 lb./hr of coal. The low Btu fuel is supplied at a pressure of 20 atm and a nominal temperature of 1000°F. Details of the gasifier and the hot gas cleanup system can be found in Cook *et al.* [1,2].

The turbine simulator includes: a low Btu gas fuel nozzle; a modified GE MS6000 combustor liner; a film cooled, first stage LM6000 nozzle assembly, and an impingement cooled transition piece. A GE MS6000 combustor liner was chosen because its fuel requirements are close to the capacity of the gasifier/HGCU system. The liner was modified to meet the air requirements of low Btu fuel combustion, while the reverse flow sleeve is standard hardware. The fuel nozzle wa

designed specifically for low Btu gas combustion [3]. A film cooled LM6000 first stage nozzle was chosen to simulate the film cooled nozzles found in advanced gas turbines with high firing temperatures.

Design of the turbine simulator was initiated in April 1991. Fabrication and assembly were completed in August 1992. The current test plan includes seven fired tests with coal gas from the pilot scale gasifier/HGCU system, designated as Runs 3, 3A, 4, 5, 6, 7, and 8. This paper focuses on the results from Runs 5 and 6, which were completed in November 1993 and May 1994, respectively. The results from previous tests have been discussed by Cook *et al.* [4,5].

A recent addition to the turbine simulator is the optional ability to augment the low Btu fuel with natural gas. Because the fuel requirements of the turbine simulator slightly exceed the capacity of the gasifier/HGCU system, the heating value of the low Btu fuel must be enhanced with natural gas to reach sustained combustion exit temperatures in excess of 2100°F. The natural gas is added to the low Btu fuel far upstream of the combustor so that the blended fuel entering the turbine simulator is completely mixed. This capability was first exercised during selected time periods of Run 6. The blended fuel was less than 10% (by volume) added natural gas.

RQL Combustor

A new reduced scale RQL combustor design is nearly complete. Nominal design conditions are 0.75 lbs./sec total flow and combustor exit temperatures up to 2500°F. The RQL combustor has a modular construction, which allows for

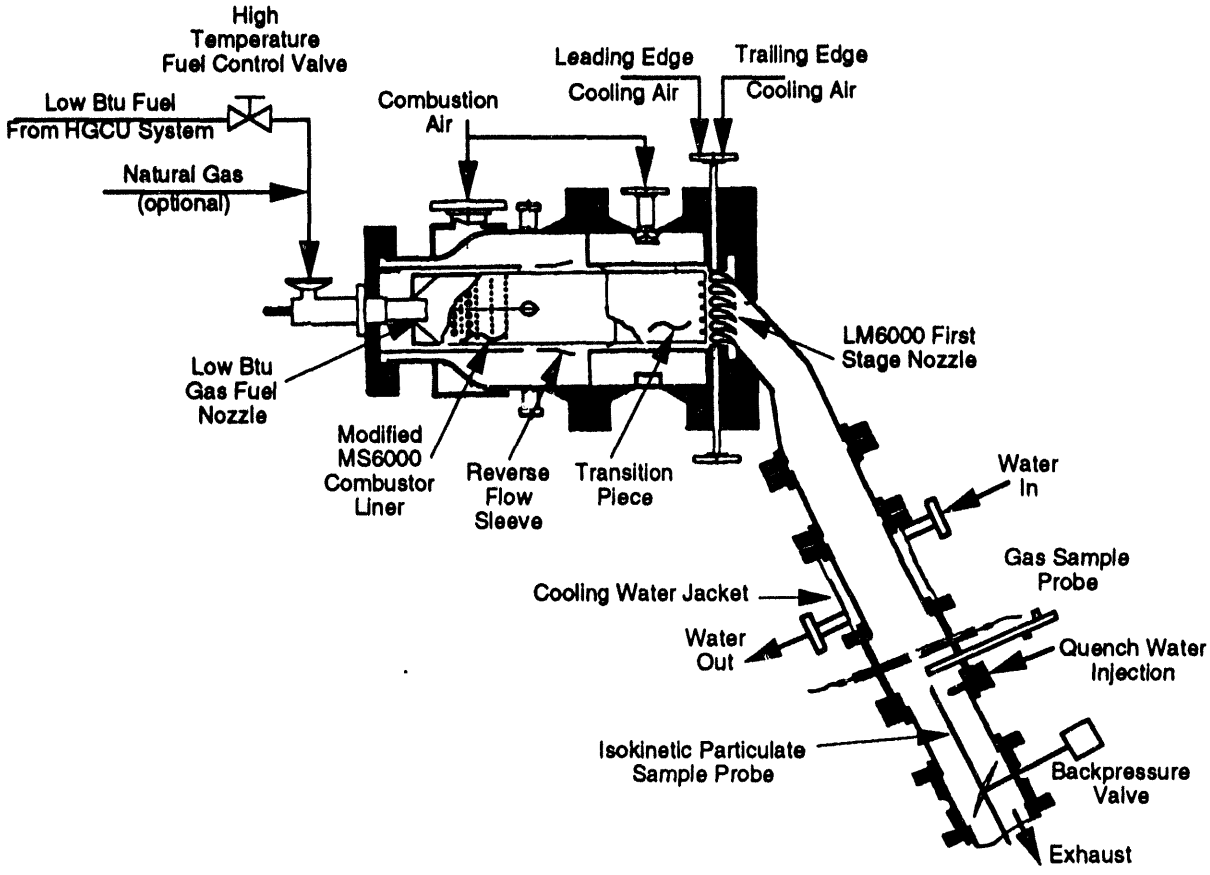

Figure 1. The Turbine Simulator Test Stand

rapid evaluation of different hardware configurations. The rich and lean stages are separate components, and the air flow to each stage can be independently varied.

Insights gathered from previous reduced scale RQL combustion tests [5], cold flow visualization tests, and computational fluid dynamics (CFD) studies have been incorporated into the new design. The new design includes a converging rich stage to separate the fuel rich and fuel lean combustion zones, and a backward facing step at the inlet to the lean stage for flame stabilization. The converging cone has been added to the tail end of the rich stage to close the rich stage recirculation zone. The reduction in diameter also accelerates the flow and helps prevent upstream flow of quench air into the rich stage.

RESULTS

The turbine simulator was fired with coal gas for 41 hours during Run 5 and 67 hours during Run 6, for a total of 179 hours of fired operation over 5 tests. The gasifier was fueled with Illinois #6 coal for both Runs 5 and 6. A typical fuel composition (after H_2S removal) is given in Table 1. During Run 5, the turbine simulator was operated at a combustor exit temperature of 2300°F for the first time. In addition, the low Btu fuel and burned gas were sampled for trace elements in both the solid phase and the vapor phase. Radian Corporation assembled and operated the trace element sample trains, and also performed all trace element sample analyses. Deposits were collected from several locations within the turbine simulator at the conclusion of Run 5 and were also analyzed for trace elements.

The turbine simulator reached a combustor exit temperature of 2500°F, representative of GE "F" class gas turbines, for the first time during Run 6. An on-line atomic emission spectrometer, developed at Ames Laboratory, was also used to measure vapor phase alkali species concentrations in the hot low Btu fuel.

Wall Temperatures

Except for the head end of the combustor, metal wall temperatures throughout the turbine simulator (including the transition piece and film-cooled cascade) have been within design specifications for all of the long duration tests. However, metal wall temperatures at the head end of the combustor frequently have exceeded design limits. As a result, sections of the cap/cowl were damaged during three of the first four long duration tests. An improper fuel/air ratio at the head end of the combustor was probably the largest single factor which contributed to the high wall temperatures.

After Run 5, during which the cap/cowl was again damaged by high metal wall temperatures, several modifications were made to the fuel nozzle and combustor liner. First, a small step between the fuel nozzle assembly and the cap/cowl was eliminated by bringing the fuel nozzle forward. Second, the swirl angle on the fuel side of the fuel nozzle was reduced from 40 degrees to 15 degrees. Finally, the first two rows of mixing holes in the combustor liner were

Table 1. Typical Pilot Plant Low Btu Fuel Composition

Species	Mole Percent
CO	8.6
H_2	17.3
CH_4	2.7
N_2	30.1
CO_2	12.6
H_2O	28.0
Ar	0.3
NH_3	0.4
TOTAL	100.0

AIIM

Association for Information and Image Management

1100 Wayne Avenue, Suite 1100
Silver Spring, Maryland 20910

301/587-8202

Centimeter

Inches

MANUFACTURED TO AIIM STANDARDS
BY APPLIED IMAGE, INC.

4 of 6

closed to increase the fuel/air ratio at the head end of the combustor. These changes were designed to reduce recirculation of hot burned gas towards the cap/cowl and to move the combustion zone downstream, away from the cap/cowl.

The effectiveness of these hardware changes was demonstrated during Run 6. Cap/cowl temperatures never exceeded 1000°F, even at combustor exit temperatures as high as 2500°F. The hardware modifications also resulted in significantly lower combustor liner temperatures.

Emissions

The fuel nozzle and combustor liner modifications had little effect on NO_x emissions (see Figure 2). The slightly higher NO_x emissions seen in Run 6 can be attributed to a slightly higher NH_3 content in the fuel. The average NH_3 concentration in the low Btu fuel was 4100 ppmv during Run 5, while the average NH_3 concentration was 4400 ppmv during Run 6. The emissions measurements shown in Figure 2 (and all of the emissions measurements reported in this paper) were taken when the turbine simulator was fueled solely with low Btu gas.

Figure 2 shows NO_x emissions tend to decrease as the combustor exit temperature increases. At 2300°F, NO_x emissions averaged 180 ppmv (on a dry, 15% O_2 basis) during Run 5, representing a conversion of NH_3 to NO_x of about 20%. At a combustor exit temperature of 1600°F, NO_x emissions averaged 300 ppmv (on a dry, 15% O_2 basis) during Run 6, representing a conversion of NH_3 to NO_x of about 30%. The decrease in NO_x as exit temperature increases is primarily due to the increasing equivalence ratio at the head end of the combustor.

The combustor liner and fuel nozzle modifications made to decrease cap/cowl temperatures were expected to cause an increase in CO emissions. Figure 3 shows the increase was relatively small. CO emissions were below the detection limit of about 1 ppmv (on a dry, 15% O_2 basis) at combustor exit temperatures above 2100°F. CO emissions increased as the combustor exit temperature decreased, and CO emissions increased more rapidly with the modified hardware. UHC emissions also increased as the combustor exit temperature decreased (see Figure 4).

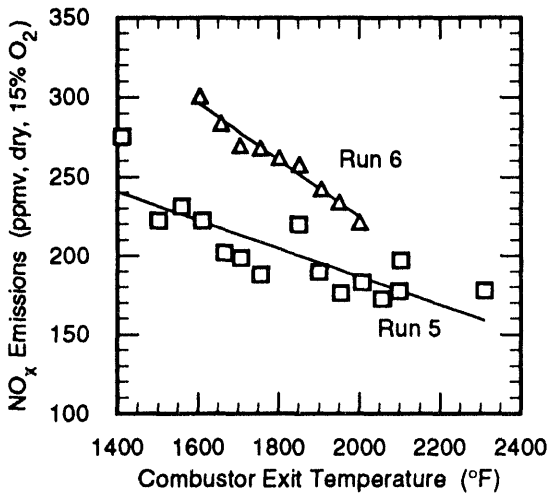

Figure 2. Turbine Simulator NO_x Emissions

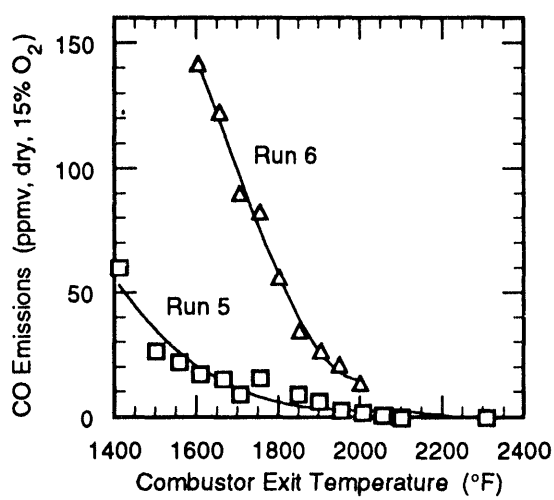

Figure 3. Turbine Simulator CO Emissions

Fuel Alkali Levels

During Run 6, vapor phase alkali concentrations were measured with the Ames Alkali Monitor, an on-line atomic emission spectrometer developed by Ames Laboratory [6]. Low Btu fuel was sampled isokinetically just upstream of the turbine simulator and then filtered before being sent to the alkali monitor. Although the low Btu fuel exited the HGCU system at about 1000°F, the fuel cooled to about 860°F at the alkali sample location. The sample line and filter were maintained at a temperature of about 950°F.

The results of the vapor-phase alkali measurements are shown in Table 2. The alkali monitor was unable to observe any vapor phase potassium above the detection limit of about 1 ppb by weight as K. Vapor phase sodium concentrations averaged about 3 ppb, with a maximum of approximately 5 ppb by weight as Na.

Also shown in Table 2 are chemical equilibrium calculations of expected vapor-phase alkali species concentrations at two coal gas temperatures. The calculations were performed with a modified version of CET89, the NASA chemical equilibrium code [7]. The coal gas composition listed in Table 1 was used for the calculations, with the addition of 200 ppmv HCl, 2500 ppmv H_2S, and sufficient amounts of sodium and potassium to insure the existence of condensed sodium and potassium species in the equilibrium mix.

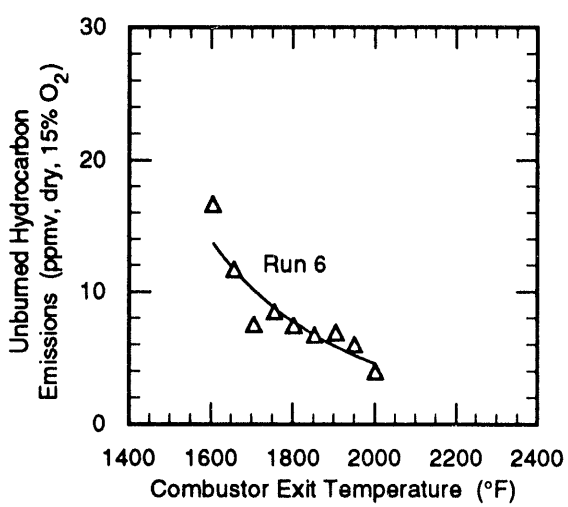

Figure 4. Turbine Simulator UHC Emissions

The two principal sources of thermodynamic data were the JANAF tables [8] and the extensive compilation of Barin [9]. Approximately 60 solid, liquid, and vapor sodium and potassium species were considered. Only the most abundant alkali species are listed in Table 2; all other alkali species were present in the vapor phase at concentrations below 0.01 ppb by weight as Na or K. Solid carbon (coke) was deliberately excluded from the equilibrium composition, based on kinetic constraints. Sodium and potassium silicates and aluminates were also excluded for similar reasons.

Table 2 shows the measured total vapor phase sodium concentration is within the range of the equilibrium calculations, assuming a coal gas temperature of between 850°F and 1000°F. Alkali species concentrations were calculated at two temperatures because of the uncertainty in the fuel temperature. As the low Btu gas in the main fuel line cooled from 1000°F to 860°F, some of the vapor phase alkali may have condensed on the surface of entrained particles. This condensed material may have been partially (or fully) volatilized when the sample gas was heated in the sample line and/or when the particles came to rest on the heated particulate filter.

At these temperatures, both the measured and calculated vapor phase alkali levels are well within gas turbine limits (20 ppb by weight total alkali in the products of combustion). The bulk of the sodium is expected to exist in the solid phase as sodium carbonate (Na_2CO_3) and sodium chloride (NaCl), and the bulk of the potassium is predicted to exist in the solid phase as potassium chloride (KCl). The predicted vapor phase potas-

sium concentrations shown in Table 2 are slightly higher than previously reported [5] because of refinements to the thermodynamic database and computational procedures.

The chemical equilibrium calculations were performed assuming a large excess of solid sodium and potassium compounds in the equilibrium mix. This is a good assumption for sodium, because sodium bicarbonate is injected into the low Btu fuel upstream of the HGCU system. However, this is a very conservative assumption for potassium. For this reason, the calculated equilibrium vapor phase concentration of sodium is in better agreement with the measurements than the calculated equilibrium vapor phase concentration of potassium.

Trace Elements

The turbine simulator burned gas was sampled isokinetically for vapor phase trace elements during Run 5. The burned gas was diluted 1:1 with nitrogen and then cooled to approximately 250°F before being filtered according to EPA Method 5. A portion of the sample gas was then passed through the impinger train specified in EPA Method 29. Three vapor phase trace element samples were collected using this technique. Two blank samples, collected during a period when low Btu fuel was not available, were obtained by establishing normal air flows through the simulator and sampling according to the above procedure.

Table 3 shows the average concentration of each element detected in the vapor phase burned gas samples. Element concentrations were determined by GFAAS (Graphite Furnace Atomic Absorption Spectrophotometry), ICPES (Inductively Coupled Plasma Emission Spectroscopy), or CVAAS (Cold Vapor Atomic Absorption Spectrophotometry). Ten other elements (aluminum, antimony, beryllium, cobalt, copper, magnesium, molybdenum, phosphorus, potas-

Table 2. Comparison of Measured and Equilibrium-Modeled Vapor Phase Alkali Concentrations in Low Btu Fuel

	Gas Phase Concentration (ppb by weight as Na or K)		
	Equilibrium Model Calculations		Measurements
Gas Phase Species	T = 850°F	T = 1000°F	T = 860°F
Na	<0.01	<0.01	
NaCl	0.1	4.3	
NaOH	<0.01	<0.01	
$(NaCl)_2$	0.03	1.9	
Total Na	0.13	6.2	3
K	<0.01	<0.01	
KCl	0.5	19.6	
KOH	<0.01	0.01	
$(KCl)_2$	0.1	7.6	
Total K	0.6	27.2	<1

sium, and vanadium) were below the detection limit in all the burned gas samples.

The presence of relatively volatile elements (such as arsenic, mercury, and selenium) in the vapor phase samples is not surprising. Even at an exhaust gas temperature as low as 250°F, these elements might be expected to remain in the vapor phase. The detection of relatively non-volatile elements (such as iron and and manganese) suggests the vapor phase samples were contaminated with a small amount of particulate matter. In particular, the concentration of sodium in the vapor phase samples is greater than expected, based on the measured amount of condensed-phase and vapor-phase sodium in the fuel. The relatively large amount of sodium in the blank samples indicates the blank samples were also contaminated with some sodium containing condensed matter.

RQL Combustor

Figure 5 shows the velocity vectors calculated by a two-dimensional CFD analysis of the new RQL combustor rich stage. The strong swirl generated by the fuel nozzle creates a central recirculation zone and a corner recirculation zone at the head end of the rich stage. There is also another weak recirculation zone, near the wall of the converging section, which extends most of the length of the rich stage. Without a converging section the rich stage recirculation zone would extend to the point of quench air injection, and quench air would be drawn into the rich stage.

Table 3. Vapor Phase Emissions of Trace Elements

	Concentration in Turbine Simulator Exhaust ($\mu g/Nm^3$)	
Element	Burned Gas	Blank Sample
Arsenic	16	BDL
Barium	6.0	1.4
Cadmium	0.4	BDL
Calcium	70	44
Chromium	40	2.0
Iron	1440	13
Lead	3.2	1.1
Manganese	280	24
Mercury	4.0	0.6
Nickel	52	7.9
Selenium	1.2	0.8
Sodium	120	61
Titanium	2.0	BDL
Zinc	32	6.6

BDL = below detection limit

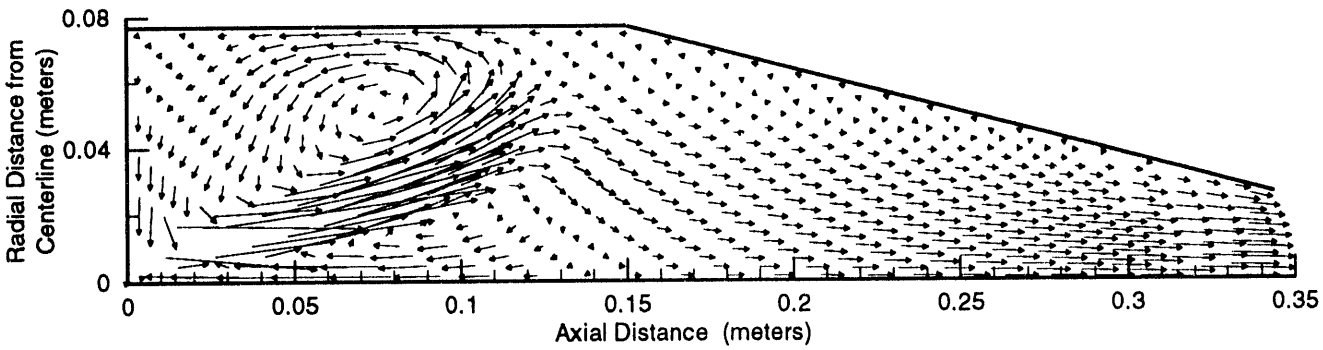

Figure 5. Computed Velocity Vectors in Rich Stage of RQL Combustor

FUTURE WORK

One additional long duration test of the turbine simulator is scheduled for 1994. A new low Btu fuel nozzle design, incorporating a radial air swirler, will be used in this test. The cap/cowl will have to be modified to accept the new fuel nozzle, since the new nozzle has a significantly smaller overall diameter than the current nozzle. Fuel nozzle performance will be evaluated by measuring NO_x, CO, and UHC emissions, as well as combustor liner and cap/cowl temperatures. After the test, the nozzle will be examined for deposits and signs of erosion.

Design of the new reduced scale RQL combustor is nearly complete. Initial tests will be conducted using natural gas/nitrogen/ammonia blends for fuel. A reduced scale RQL combustion test with a slip stream of low Btu fuel from the pilot plant gasifier/HGCU system is also scheduled for 1994. The information gathered from these tests will be used to design a larger scale (turbine simulator scale) RQL combustor.

REFERENCES

1. Cook, C. S., E. Gal, A. H. Furman, and R. Ayala. 1992. Integrated Operation of a Pressurized Fixed Bed Gasifier and Hot Gas Desulfurization System. In *Proceedings of the Twelfth Annual Gasification and Gas Stream Cleanup Systems Contractors Review Meeting*, 84-94. DOE/METC-92/6128. NTIS/DE93000228. Springfield, VA: National Technical Information Service.

2. Cook, C. S., E. Gal, A. H. Furman, and R. Ayala. 1991. Integrated Operation of a Pressurized Fixed Bed Gasifier and Hot Gas Desulfurization System. In *Proceedings of the Eleventh Annual Gasification and Gas Stream Cleanup Systems Contractors Review Meeting*, 45-55. DOE/METC-91/6123. NTIS/DE92001101. Springfield, VA: National Technical Information Service.

3. Lawson, C. C. *Water-Cooled Components Test Program, Final Report.* 1985. DOE/MC/20192-1953. Contract DE-AC21-83MC20192.

4. Cook, C. S., N. Abuaf, A. S. Feitelberg, S. L. Hung, D. J. Najewicz, and M. S. Samuels. 1993. Combustion Tests of a Turbine Simulator Burning Low Btu Fuel and a Rich-Quench-Lean Combustor. In *Proceedings of the Coal-Fired Power Systems 93 — Advances in IGCC and PFBC Review Meeting*, 169-178. DOE/METC-93/6131. NTIS/DE93000289. Springfield, VA: National Technical Information Service.

5. Cook, C. S., N. Abuaf, A. S. Feitelberg, S. L. Hung, D. J. Najewicz, and M. S. Samuels. 1993. Combustion Tests of a Turbine Simulator Burning Low Btu Fuel From a Fixed Bed Gasifier. In *Proceedings of the Joint Contractors Meeting: FE/EE Advanced Turbine Systems Conference FE Fuel Cells and Coal-Fired Heat Engines Conference*, 199-208. DOE/METC-93/6132. NTIS/DE93011308. Springfield, VA: National Technical Information Service.

6. Haas, W. J., Jr., D. E. Eckels, S. H. D. Lee, W. M. Swift, L. H. Cowell, M. D. Stephenson, and R. T. LeCren. 1991. Alkali Monitoring for Direct Coal-Fired Turbine Combustors. In *Proceedings of the Eight Annual Coal-Fueled Heat Engines and Gas Stream Cleanup Systems Contractors Review Meeting*, 360-371. DOE/METC-91/6122. NTIS/DE91002091. Springfield, VA: National Technical Information Service.

7. McBride, B. J. 1989. *CET89 – Chemical Equilibrium with Transport Properties.* University of Georgia: Computer Software Management and Information Center.

8. Barin, I. 1989. *Thermochemical Data of Pure Substances.* New York: VCH.

9. Chase, M. W., C. A. Davies, J. R. Downey, Jr., D. J. Frurip, R. A. McDonald, and A. N. Syverud. 1985. *JANAF Thermochemical Tables, Third Edition.* Journal of Physical and Chemical Reference Data, 14, Supplement 1.

7.3 Advanced Turbine Systems Program Overview

Holmes A. Webb
Morgantown Energy Technology Center

ABSTRACT

The U.S. Department of Energy's (DOE) Office of Fossil Energy and Office of Energy Efficiency & Renewable Energy are jointly supporting a program to develop Advanced Turbine Systems (ATS). Demonstrations of commercial prototypes will be completed by the year 2000 for both utility- and industrial-scale applications. The systems will exhibit the following characteristics:

- **Ultra-high efficiency** (Utility systems: greater than 60 percent [lower heating value basis]/industrial systems: greater than 15 percent improvement over today's best technology),
- **Environmental superiority** (single digit NOx and reduced carbon dioxide, carbon monoxide, and unburned hydrocarbons),
- **Cost competitiveness** (10 percent lower cost of electricity),
- **Reliability, Availability, and Maintainability (RAM)** equivalent to today's best systems.

The program is primarily directed toward natural gas utilization, but eventual application of the technology to coal-fired systems is not overlooked. In major procurements, contractors are required to address (in paper studies though not in testing) the eventual adaptation of their systems to coal firing. Another program element targets the transfer of ATS technology to coal-fired turbine systems being funded by DOE, such as integrated gasification combined cycle, pressurized fluidized bed combustion, and externally fired combined cycle.

Implementation of the program is proceeding well. Phase I systems studies have been completed, and Phase II concept development has been underway for about a year. Release of solicitation for Phase III proposals has been announced for July, 1994. This phase of the program will see teams led by turbine manufacturers move into full scale testing of critical components. Generic research and development has been proceeding in parallel with the major development effort. METC has started testing in their Advanced Turbine Combustion test facility, and Oak Ridge National Laboratory has initiated a materials test program. The industry/university consortium established by the South Carolina Energy Research and Development Center has completed their second round of university awards, with 23 university projects now underway.

Support for this $700 million program has been strong, and budgets have been consistent with those outlined in a Report to Congress on the program. Funding was about $28 million in FY 94, and the President's budget for FY 95 includes $65 million for ATS.

Poster Session

P1 High Temperature Electrochemical Separation of H_2S from Coal Gasification Streams

CONTRACTOR INFORMATION

Contract Number	DE-FG22-91PC91288
Contractor	Georgia Institute of Technology School of Chemical Engineering Atlanta, Georgia 30332-0100 (404) 894-2839
Contractor Project Manager	E. Faith Gleason
Principle Investigator	Jack Winnick
METC Project Manager	Kamalendu Das
Period of Performance	October 1, 1991 - November 30, 1994

OBJECTIVE

A method of polishing coal synthesis gas by an electrochemical membrane operation is being perfected. The operation takes advantage of an electrochemical potential gradient rather than conventional techniques, separating the H_2S from the coal gas stream, leaving only H_2 to enrich the exiting fuel gases. Sulfur is the by-product that is carried away by a separate inert sweep gas and condensed downstream. The technology is attractive due to simplicity as well as economics when compared to alternatives.

An analytical model describing the preferred reduction of H_2S, the transport of S^{2-}, and the competing transport of CO_3^{2-} through the removal cell has continued[11]. The main objective is the relation between cell polarization and current efficiency. This has been realized.

Recent experiments have focused on removing 100 ppm inlet H_2S, utilizing laboratory fabricated cobalt cathodes.

INTRODUCTION

A schematic of the mechanism used for electrochemical separation is presented in Figure 1. The process gas, cleansed of particulates, passes over the cathode. Here the best Lewis acid, electron acceptor, will be reduced. In this case H_2S is favored, resulting in the following:

$$H_2S + 2e^- \rightarrow S^{2-} + H_2 \qquad (1)$$

The sulfide ions are transported, by migration and diffusion, across the membrane. Once the sulfide ion reaches the anode side, oxidation to elemental sulfur occurs by the following:

$$S^{2-} \rightarrow 1/2\, S_2 + 2e^- \qquad (2)$$

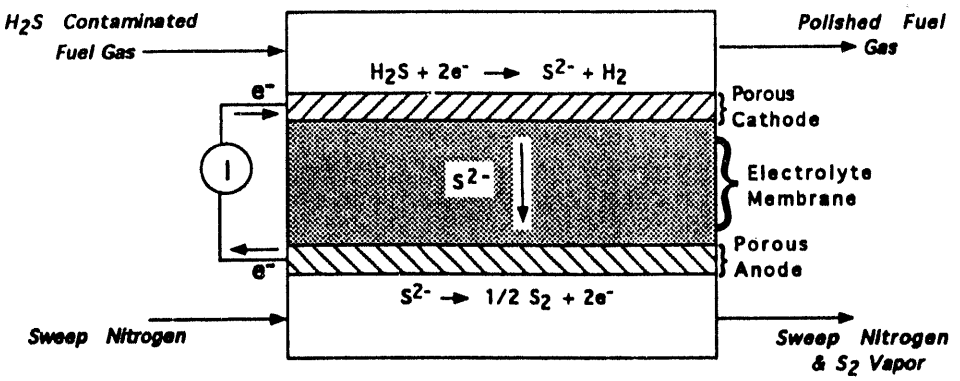

Figure 1. Schematic of Electrochemical Cell

The vaporous sulfur is condensed downstream.

Processes to remove H_2S typically rely on low-to-ambient temperature adsorption, followed by sorbent regeneration and Claus plant treatment for conversion of H_2S to a salable by-product, sulfur. Although effective, this type of removal is very process-intensive as well as energy-inefficient due to low temperature operation. Gasification streams generally range from 500°C - 1000°C, requiring cooling before and reheating after process gas sweetening. Although these technologies have proven capable of meeting H_2S levels required by MCFC, there are several disadvantages inherent to these processes[7,8].

Alternative high temperature methods are presently available, but process drawbacks including morphological changes in catalytic beds[9] or inefficient molten salt sorbent processes[10] negate savings incurred through energy efficient removal temperatures.

An electrochemical membrane separation system for removing H_2S from coal gasification product streams is the subject of this investigation. The high operating temperature, flow-through design, and capability of selective H_2S removal and direct production of elemental sulfur offered by this process provide several advantages over existing and developmental H_2S removal technologies. The remaining factor is a thorough economic evaluation asserting the viability of the process.

An initial economic evaluation[11] showed the process noteworthy. Further analysis will require developing an analytical model describing 1) the preferred reduction of H_2S among competing reactants in the gasification stream, 2) the transport of S^{2-} through the electrolyte filled membrane, and 3) competing transport of CO_2 through the removal cell. The model can give the maximum current efficiency for H_2S removal, depending on variables such as flow rate, temperature, current application, and total cell potential. Extended application of the model will predict cell performance under varying cell currents, gas compositions and flow rates. It will also permit economic projection in various applications.

Analytical Model

A theoretical model based on applied current, flow rate, and electrochemical effects has been investigated, relating anode CO_2 production with % H_2S removal. Although the model is not completed, adequate power estimates for percentage removals of H_2S can be computed.

Preferential Reduction of H_2S.

H_2S has been shown to be readily reduced in hot gas mixtures, even at low ppm levels. The situation is complicated when coal gas mixtures are processed. Carbon dioxide and water vapor compete in the reduction reaction at the cathode by:

$$CO_2 + H_2O + 2e^- \Rightarrow CO_3^{2-} + H_2 \quad (3)$$

The ionic flux through the membrane depends on the relative mobility of carbonate and sulfide ions as well as their concentrations.

Preventing the oxidation of carbonate at the anode is necessary for prohibiting its transport through the membrane, the desired anodic reaction being:

$$S^{2-} \Rightarrow 1/2\ S_2 + 2e^- \quad (2)$$

This occurs at a standard potential some 700 mV lower than the oxidation of carbonate:

$$CO_3^{2-} \Rightarrow CO_2 + 1/2\ O_2 + 2e^- \quad (4)$$

Summing the half-cell reactions (**1**) and (**2**) results in the following overall reaction at 923K:

$$H_2S \Leftrightarrow H_2 + 1/2\ S \quad (5)$$
$$E_a^o = -0.239\ V$$

and when the half-cell reactions (**3**) and (**4**) are summed:

$$H_2O \Leftrightarrow H_2 + 1/2\ O_2 \quad (6)$$
$$E_b^o = -1.030\ V$$

The relative extent of each of these reactions is determined by chemical equilibrium. Each will occur at the *same cell potential*; but as expressed by the Nernst relation, the concentration terms will be greatly affected by the large difference in the standard cell potentials, E^o, values.

$$E = E_a^o - \left(\frac{RT}{nF}\right) \ln \left\{ \frac{a_{S^{2-}_{cath}} P_{H_2\,cath} P^{\frac{1}{2}}_{S_2\,an}}{a_{S^{2-}_{an}} P_{H_2S_{cath}}} \right\} \quad (7)$$

$$E = E_b^o - \left(\frac{RT}{nF}\right) \ln \left\{ \frac{a_{CO_3^{2-}_{cath}} P_{H_2\,cath} P_{CO_2\,an} P^{\frac{1}{2}}_{O_2\,an}}{a_{CO_3^{2-}_{an}} P_{CO_2\,cath} P_{H_2O_{cath}}} \right\} \quad (8)$$

We here assume a process gas is supplied to the cathode with an H_2S level of 100 ppmv, a CO_2 level of 14.2%, and an H_2O level of 5.7%, and that 90% of the H_2S is to be removed via reaction (**1**). There exists an activity ratio of $\frac{a_{CO_3^{2-}}}{a_{S^{2-}}}$ on the order of 10^5 in the anolyte, assuming equivalent electrode kinetics[5,6] for the two reactions, before a significant amount (e.g. 1%) of the carbonate is oxidized. When compared to the activity ratio of $\frac{a_{CO_3^{2-}}}{a_{S^{2-}}}$ in the catholyte of 3000, this shows the huge thermodynamic preference for the oxidation of S^{2-} to elemental sulfur by equation (**2**).

The net effect, under these conditions, is continuous and selective removal of H_2S from the process gas accompanied by enrichment of the process gas with H_2 and direct generation of elemental sulfur at the anode.

Electrical Power Requirements.

The power to drive the electrochemical membrane separator is a direct function of the potential required to drive the removal cell multiplied by the current carried by the sulfide ions across the membrane.

Power=(CellPotential) *(Cell Current) (9a)

Estimation of the current carried by the removal cell is straight-forward since two faradays of charge are carried by each mole of sulfide transported (or each mole of H_2S removed). Calculation of the cell potential is outlined below.

Along with the Nernst relation, additional energy is required to operate the separation cell due to irreversible losses. These losses occur by internal resistance, concentration effects in the process gases, and the activation barrier for electron transfer. The result is the total cell potential increasing over the reversible potential[1].

Ohmic Polarization:

Ohmic losses occur due to resistance in ionic and electronic transfer of current through the separation system. The ohmic losses can be expressed by:

$$\eta_{ohm} = IR \qquad (9)$$

with **I** representing current and **R** the total cell resistance.

Concentration Polarization:

Concentration polarization originates from developing concentration gradients due to consumption of electro-active species at the electrode surface. Transport of these species is composed of four steps, occurring in series: 1) the H_2S must diffuse through the gas-phase boundary layer to the cathode interface, 2) it must diffuse through the pores of the electrode to the electrolyte film, 3) the sulfide ion must migrate to the anode, and 4) the oxidized species must diffuse out into the sweep gas at the anode. The effect of step 3 has been minimized due to proper membrane design and steps 2 and 4 have been found to be of no consequence[2]. The limiting process for removal is thus diffusion of electro-active species to the electrode pores from the bulk gas. Since the gas-phase concentration of H_2S changes along the length of the channels, a log-mean average is used in the calculation of limiting current density by:

$$i_L = nFk_m\rho\frac{(y_{inlet} - y_{exit})}{\ln\left(\frac{y_{inlet}}{y_{exit}}\right)} \qquad (10)$$

where **n** is the number of electrons transferred per mole of species removed, **F** is Faraday's constant, $\mathbf{k_m}$ is mass transfer coefficient, ρ is the molar density of the bulk gas, and $\mathbf{y_x}$ is the inlet and exit mole fraction of H_2S. The average mass transfer coefficient was derived from an estimated Sherwood number dependent on channel dimension and constant H_2S surface concentration[3] given by:

$$N_{Sh} = \frac{k_m D_{eq}}{D_{ab}} \qquad (11)$$

with $\mathbf{D_{eq}}$ defined as the equivalent channel diameter above the electrode surface:

$$D_{eq} = 4r_h = \frac{4(\text{cross-sectional area})}{(\text{wetted perimeter})} \qquad (12)$$

and $\mathbf{D_{ab}}$ the diffusion coefficient of H_2S through the predominant species by volume in the bulk according to[4]:

$$D_{ab} = \frac{0.0018583T^{\frac{3}{2}}}{P\sigma_{ab}\Omega_{D_{ab}}}\sqrt{\frac{1}{M_a} + \frac{1}{M_b}} \qquad (13)$$

therefore, concentration overpotential is expressed in terms of applied current by:

$$\eta_{conc} = \frac{RT}{nF}\ln\left(1 - \frac{i}{i_l}\right) \qquad (14)$$

Activation Polarization:

The activation polarization at both cathode and anode is related to the rates of electrochemical reactions occurring at these electrodes. The

expression relating the kinetics of these electrode reactions is the Butler-Volmer equation:

$$i = i_o\left[\exp\left(\frac{\alpha_a F\eta_{act,a}}{RT}\right) - \exp\left(\frac{-\alpha_c F\eta_{act,c}}{RT}\right)\right] \quad (15)$$

which holds for specified temperature, pressure, and concentration of reacting species. The transfer coefficients α_a and α_c sum to the number of electrons transferred in the reaction:

$$\alpha_a + \alpha_c = n \quad (16)$$

Cell Voltage:

Total cell voltage incorporating *ohmic*, *concentration*, and *activation* overpotentials along with the Nernstian effects (7) sums to:

$$V_{cell} = \Delta E_{c-a} - |\eta_{conc}| - |\eta_{act}| - \eta_{ohmic} \quad (17)$$

where ΔE_{c-a} is the total cathode-to-anode cell voltage.

The results exhibited in Figure 2, 3, and 4 were generated using this analytical approach. The run conditions assumed equal cathodic and anodic flow rates of (200 cc/min) (the calculated results are independent of anode sweep gas flow rate), atmospheric system pressure, a run temperature of 650 °C, and three order of magnitude changes in H_2S removal (1000 ppm to 1 ppm). The cathodic and anodic exchange current densities were estimated at 40 mA/cm^2 after the results of the free electrolyte studies[5,6]. The exchange coefficients, α_a and α_c, were assumed to be unity. Ohmic resistance across the cell was conservatively estimated to be 1 Ω, based on Molten Carbonate Fuel Cell (MCFC) results[1]

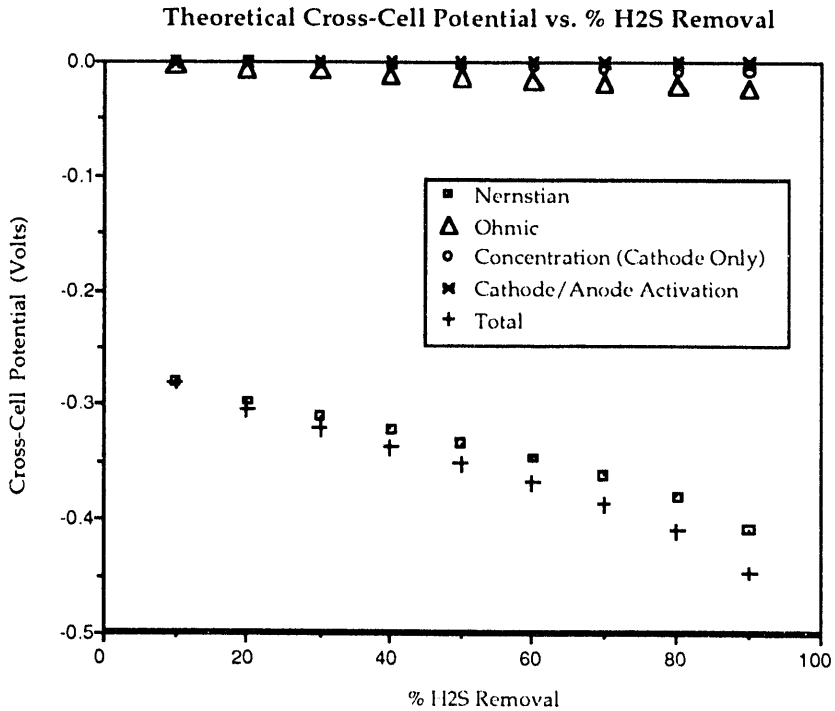

Figure 2. Theoretical Cross-Cell Potential vs. % H_2S Removal; 1000 ppm inlet

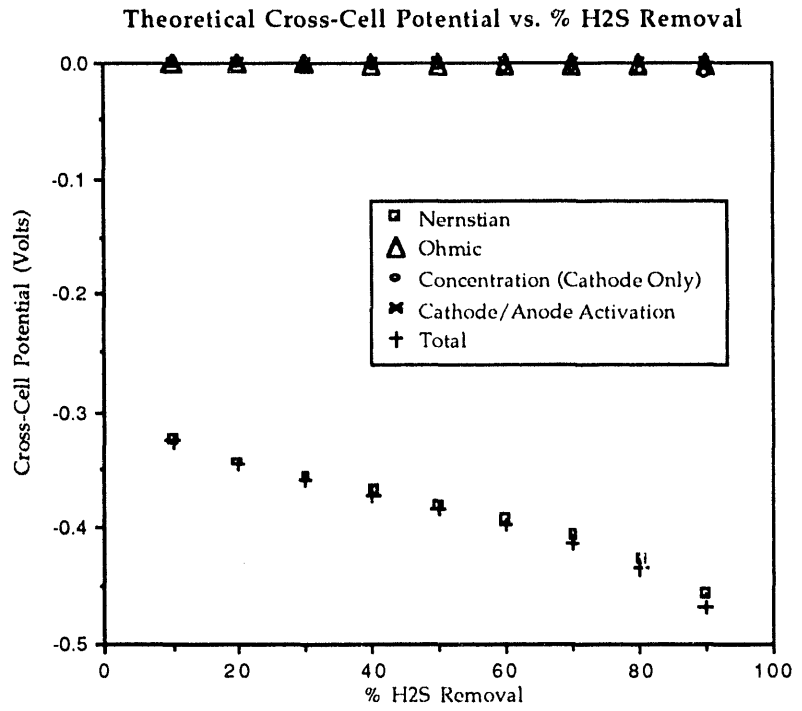

Figure 3. Theoretical Cross-Cell Potential vs. % H_2S Removal; 100 ppm inlet

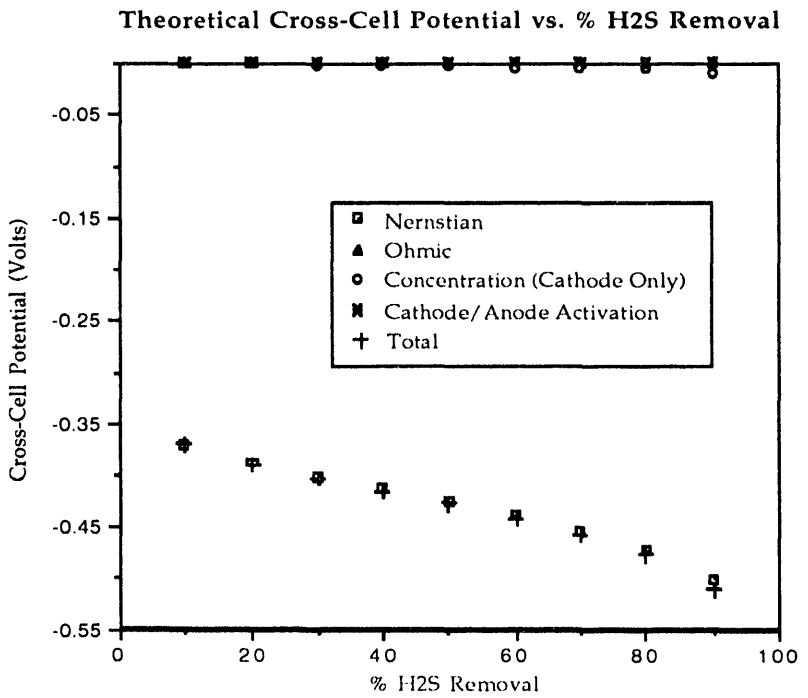

Figure 4. Theoretical Cross-Cell Potential vs. % H_2S Removal; 10 ppm inlet

These results show the activation overpotentials at both cathode and anode are negligible. This shows extremely rapid electrochemical kinetics as compared to diffusion effects from the bulk gas phase and through the electrolyte filled membrane. Cross-cell potentials are shown as the sum of the Nernstian, concentration, and ohmic polarization effects. Therefore, at 90% removal H_2S (1000 ppm - 100 ppm; 100 ppm - 10 ppm; 10 ppm to 1 ppm), the data of Figure 2, 3, and 4 show total cross-cell potentials of -0.4474 V, -0.4675 V, and -0.5107 V, which agree well with experimental cross-cell potentials. Total power requirements for these removals from (**9a**) are 10.5 W, 1.09 W, and 0.12 W (not considering current loss from anodic CO_2 production).

Parallel Sulfide, Carbonate Transport.

Since the carbonate transport of reaction (**6**) parallels the sulfide transport of reaction (**5**), the same current is available for transport of both species. Therefore, only a certain amount of current will act to transport either constituent giving a finite maximum current efficiency with respect to H_2S removal for any percentage of H_2S removed. This is dependent on gas composition and total cross-cell potential required for the desired separation of H_2S. Once the total cross-cell potential is calculated for the desired H_2S removal, the Nernst expression for transport of carbonate (**8**) can be equated to this value, since the relative extent of each occur at the same potential. The extent of parasitic CO_2 current from the removal cell associated with $\%H_2S$ removal is shown in Figure 5, 6, and 7.

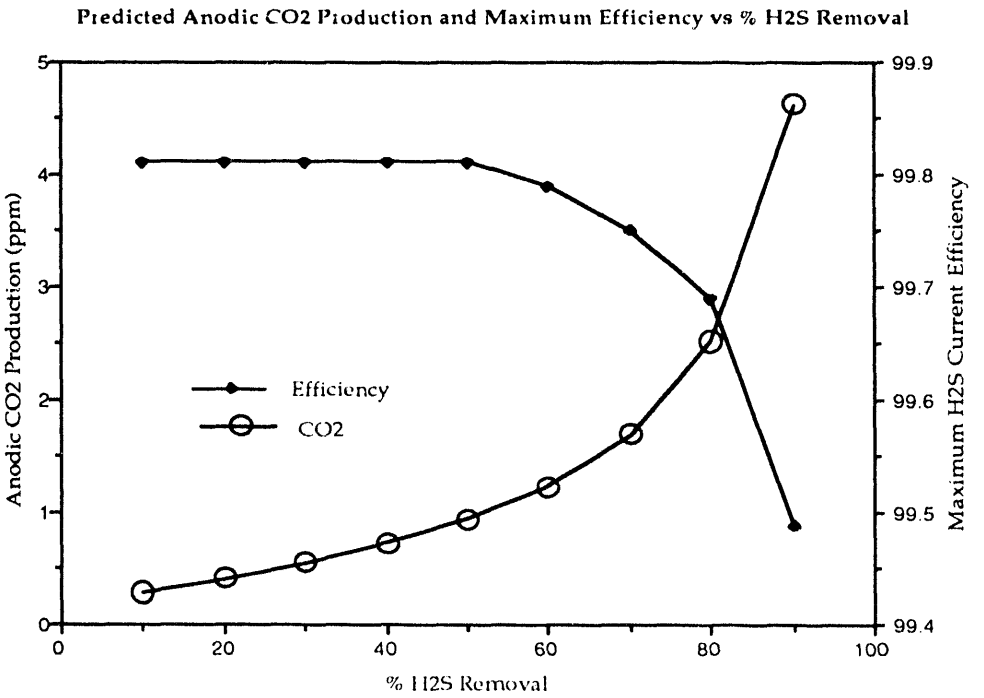

Figure 5. 1000 ppm inlet H_2S

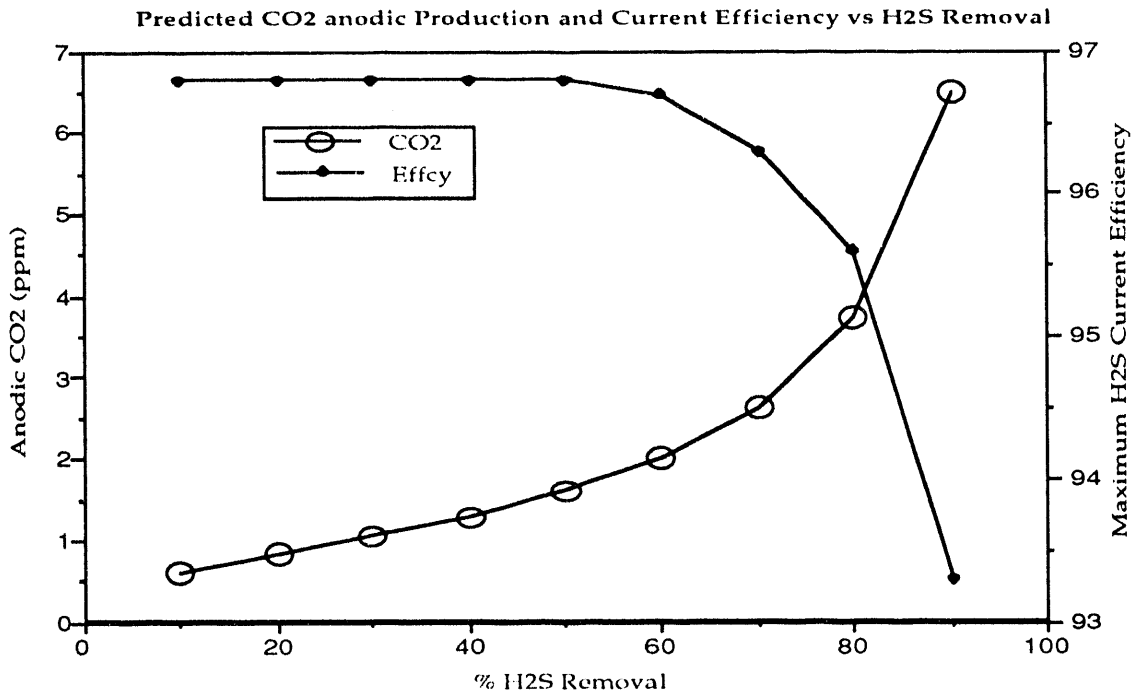

Figure 6. 100 ppm inlet H_2S

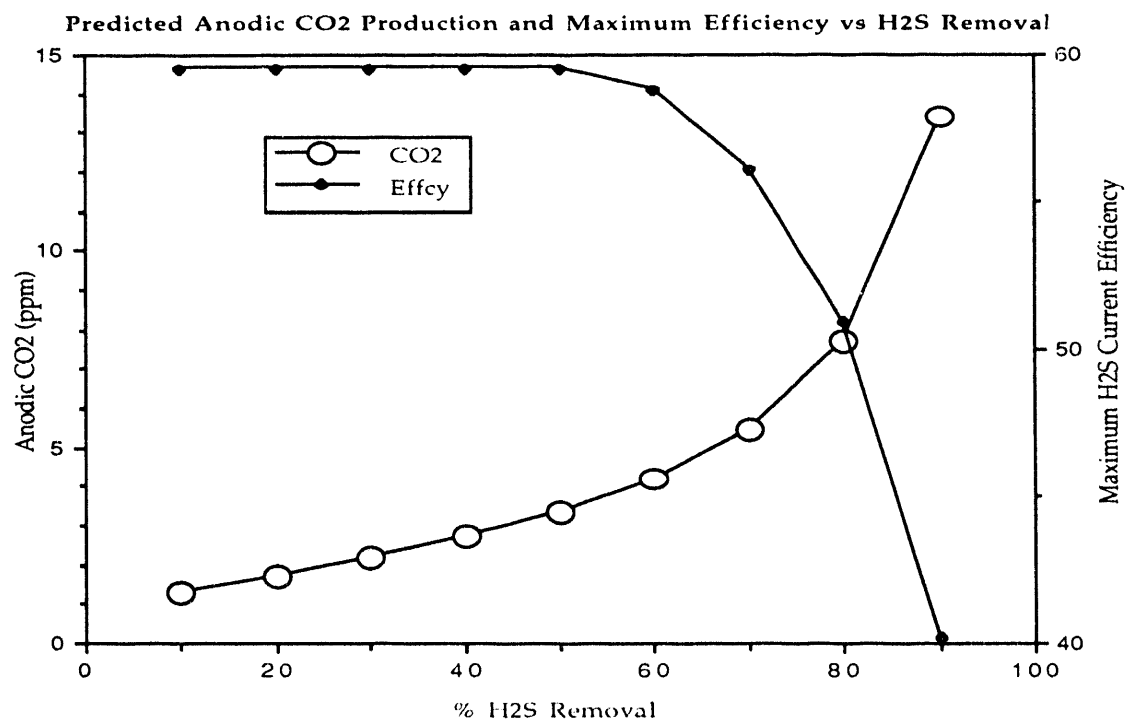

Figure 7. 10 ppm inlet H_2S

Examination of the results shows that H_2S current efficiency drops only to 99.5% at 90% H_2S removal (1000 ppm to 100 ppm H_2S), 93.2% at 90% H_2S removal (100 ppm to 10 ppm H_2S), and 40.2% at 90% H_2S removal (10 ppm to 1 ppm H_2S). The excess current goes to produce anodic CO2.

This is a favorable result considering the power requirement at higher inlet H_2S concentrations is considerably greater than at lower concentrations, Figure 8 (10.52 W at 1000 ppm inlet H_2S, 0.29 W at 10 ppm inlet H_2S); a high efficiency is a must in the higher H_2S concentrations if the process is to be economically viable. Energy requirements for the 10 ppm H_2S removal are negligible, shown in Figure 8, alleviating concern due to lower current efficiencies.

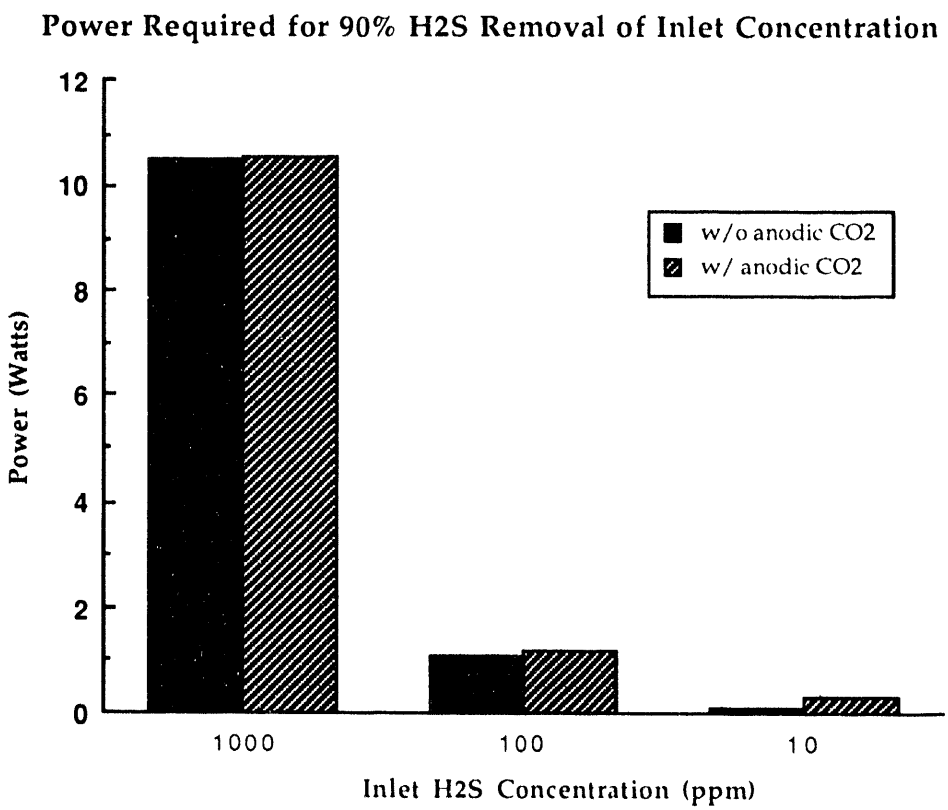

Figure 8. Power Estimates

Table I. Percentage Removal with Applied Current

I_{app} (mA)	% of Total H_2S Removed	% of Total CO_2 Removed
200	0	10
500	28	30
1000	50	50
1500	70	75

EXPERIMENTAL RESULTS

An experiment (Run#16) examining the removal capability of the EMS with cobalt cathode was recently performed The focus dealt with H_2S removal as well as containing hydrogen cross-over from the process gas side (cathode) of the membrane to the sweep gas side (anode).

Run #16

Cell materials consisted of a cobalt cathode (80% porous), the anode material remained Ni (85% porous), a stabilized zirconia membrane (66% porous), housings of MACOR (machineable ceramic), aluminum foil gasket seals, and a prepressed disk of $(Li/K)_2CO_3$ (8 grams) corresponding to the void volume in the zirconia membrane. Electrode materials were verified by x-ray diffraction, Figure 9.

Examination of the cobalt-cathode electrochemical membrane separator (EMS), produced stoichiometric CO_2 removal and addition at both cathode and anode, respectively, before addition of H_2S. After introducing H_2S to the EMS, system gases equilibrated to 10% CO_2, 18% CO, 10% H_2O, 36% H_2, 26% N_2 and 90 ppmv H_2S after the water-gas shift reaction. H_2S removal at varying currents was attempted, starting with stoichiometric current (2 mA for a flow of 158 cc/min), and increasing to 200 mA. H_2S removal did not appear significant (< 10 ppmv), with continued stoichiometric CO_2 removal at the cathode and production at the anode. Further application of current in steps from 200 mA to 1.5 A revealed percentage of total H_2S removal coincided with percentage of total CO_2 removal, shown in Table I. This trend was evidenced in past experiments with hydrogen cross-over present. Micro-cracks in the membrane that would enable hydrogen to cross from the process gas side (cathode side) to the sweep side (anode side) seem to be evident from Scanning Electron Microscopy (SEM) in pre-run analysis, Figure 11.

a)

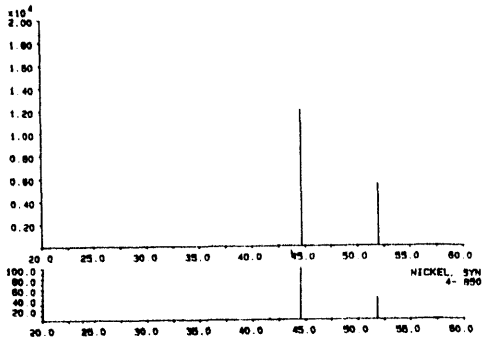

b)

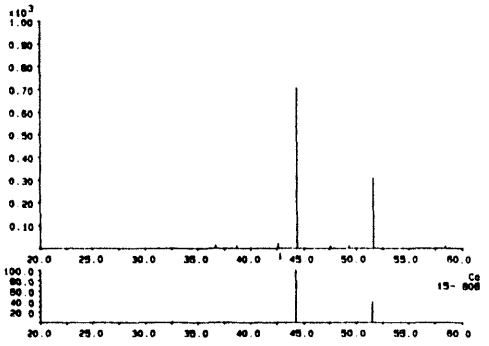

Figure 9. a) Pre-run Ni anode and b) Pre-run Co cathode

a)

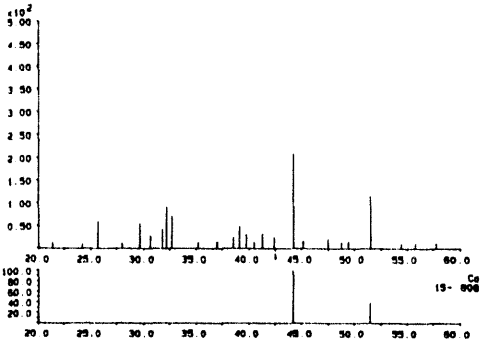

b)

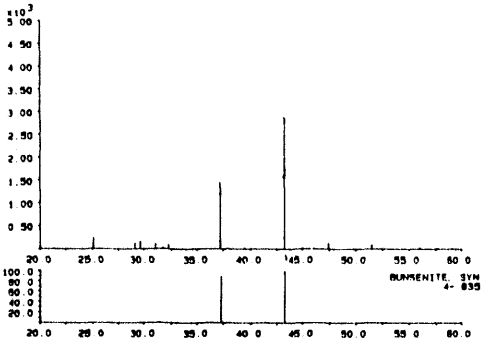

Figure 10. a.) Post-run Co cathode and b.) Post-run NiO anode

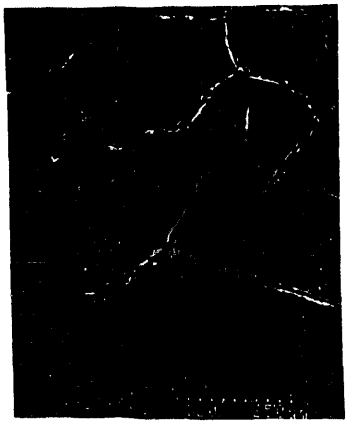

Figure 11. Scanning Electron Microscopic view of zirconia membrane.

If hydrogen cross-over occurs, two reactions are possible at the anode. One reaction is the oxidation of hydrogen and the sulfide ion to hydrogen sulfide.

$$H_2 + S^{2-} \rightarrow H_2S + 2e^-$$

Anode exit gases checked by gas chromatography showed no evidence of H_2S. The other possible reaction is the oxidation of hydrogen and carbonate to water and carbon dioxide.

$$H_2 + CO_3^{2-} \rightarrow H_2O + CO_2 + 2e^-$$

Gas chromatography did reveal minute amounts of water vapor on the anode side substantiating hydrogen cross-over. This creates loss of carbonate from the electrolyte, induces the favorability of carbonate reduction at the cathode over H_2S due in part to the higher pressure of CO_2 and H_2O available at the cathode (order of 10^5 higher than H_2S) promoting the parasitic reaction.

Favored:
$H_2S + 2e^- \rightarrow H_2 + S^{2-}$

Competing:
$H_2O + CO_2 + 2e^- \rightarrow CO_3^{2-} + H_2$

Internal resistance remained ~1 ohm.

Ineffective removal due to hydrogen cross-over forced shut-down of the cell after 76 hours of operation. Post-mortem X-ray diffraction of electrode materials revealed a conversion of the Ni cathode to NiO (bunsenite), with the cathode remaining Co, Figure 10.

SUMMARY

Initial results from the analytical model show favorable H_2S current efficiencies. Upper H_2S concentration removal resulted in a minuscule loss in current to the parasitic reaction (**6**) at 90% H_2S removal. Although the lower concentrations showed less efficiency, the amount of current needed for these removals are negligible.

The cobalt cathode used in the EMS proved stable and efficient. Removal of H_2S was deterred by the possibility of hydrogen cross-over from process gases creating alternate reactions unfavorable to the removal system. Application of back-pressure from the anode side of the cell was attempted to resolve H_2 cross-over, but proved ineffective. Examination of water vapor in the anode exit gases provided proof of the H_2 cross-over reactions parasitizing applied current.

FUTURE WORK

The main focus will be on H_2S current efficiency using a fabricated zirconia membrane with 100 ppmv H_2S fuel gas; hopefully, preventing alternate reactions due to hydrogen cross-over.

Work will continue with the analytical model; a complete economic analysis based on the completed model is the ultimate goal, if a match with real-time data exists.

REFERENCES

1. U.S. Dept. of Energy, Fuel Cell: A Handbook, DOE/METC-88/6090, Morgantown, West Virginia, 1988.

2. Kang, M. and Winnick, J., *J. Appl. Electrochem.*, **15**, 431-39 (1985).

3. Incropera, F.P., and DeWitt, D.P., Fundamentals of Heat and Mass Transfer, 2nd ed., John Wiley and Sons, New York, 1985.

4. Reid, R., Prausnitz, J., and Poling, B., The Properties of Gases and Liquids, 4th ed., McGraw-Hill, New York, 1987.

5. Banks, E., and Winnick, J., *J. Appl. Electrochem.*, **16**, 1986.

6. White, K.A., and Winnick, J., *Electrochem. Acta.*, **30**, 1985.

7. EPRIEM-1333, *Assessment of Sulfur Removal Processes for Advanced Fuel Cell Systems, Final Report,* C.F. Braun and Co., Alhambra, CA, Jan., 1980.

8. Vidt, E.J., DOE/METC DE-AC-21-81MC16220, DE82013942, Westinghouse, Dec., 1981.

9. Focht, G.D. et. al., DOE/MC/121166-2163, DE86016041, July, 1986.

10. Lyke, S.E., DOE/MC/19077-1803, DE8500961, Battelle Pacific Northwestern Laboratories, Jan. 1985.

11. Alexander, S., *PhD Thesis*, Georgia Institute of Technology, Atlanta, GA, 1992.

P2

Characterization and Fixed-Bed Testing of a Nickel-Based Hot Gas Desulfurization Sorbent

Lee D. Gasper-Galvin
Morgantown Energy Technology Center

James H. Swisher
Southern Illinois University at Carbondale

Kurt Hammerbeck
Oak Ridge Associated Universities

OBJECTIVES

The objective of this project was to (1) extend a preliminary investigation completed earlier on dispersed nickel sorbents[1] by developing new processing methods, characterizing sorbent materials more extensively, and evaluating the materials in fixed bed reactor tests, and (2) to determine the feasibility of using dispersed nickel sorbents with reductive regeneration for hot gas desulfurization.

BACKGROUND

There has been interest and active research on desulfurization of coal-derived gases since they were first produced by coal carbonization more than a century ago. A comprehensive review of the literature on metal and binary oxide sorbents was published by Swisher and Schwerdtfeger[2]. A later paper by the same authors[3] reviewed literature on mixed oxide sorbents and discussed the importance of thermodynamics in research on sulfur sorbents.

During the past 10 years, research in this field has focused on desulfurization at high temperatures because of the need for application of the technology to Integrated Gasification Combined Cycle (IGCC) systems. In the 1980's, the sorbent material receiving the most attention was zinc ferrite[4]. While it was very effective in reducing hydrogen sulfide (H_2S) concentrations in the product gas to the low ppmv level, it suffered from zinc loss due to vaporization and poor resistance to decrepitation and attrition.

More recently, zinc titanate sorbents have been shown to have comparable desulfurizing ability to zinc ferrite and to be better in durability[5-10]. There is now more research being done on zinc titanate than any other class of sorbents. However, there are still unanswered questions about its durability and reactivity over many sulfidation/regeneration cycles and its ability to serve applications in which the temperature of the gas to be desulfurized is 750°C or higher. Therefore, continuing research is justified on alternate sorbent materials.

There has been some, but not an extensive amount, of prior work on sorption of sulfur (S) by nickel (Ni) for hot gas desulfurization applications. One of the properties of nickel that is somewhat unique is that it forms a liquid sulfide at sufficiently high temperatures with high sulfur potentials or H_2S levels[11,12]. A eutectic exists in the Ni-S phase diagram at 637°C and a composition of 33.4 wt % or 21.5 wt % S[13]. Under controlled conditions, the formation of a liquid

phase can be used to advantage in hot gas desulfurization. The approach used by Steiner and Gutterman[14] was to use pellets of Ni and NiO in a fixed-bed reactor. When simulated coal gas was passed through the beds at 740°C, liquid sulfide formed and flowed away from the pellets. Thus, there was no solid sulfide present to serve as a diffusion barrier and curtail the reaction. Their concept included a provision for collecting the sulfide formed and regenerating it in a separate reactor.

Thermodynamic calculations show that the solid Ni-liquid Ni sulfide equilibrium will not reduce H_2S levels in coal gasification product gas to the low ppmv level. Fortunately, however, another mechanism can be used for sorption of S by Ni in the low concentration range. Patel, Rich, and Maru[15] showed that chemisorption of S on Ni occurs readily in the 500 to 700°C temperature range. They evaluated ten commercial catalysts containing dispersed Ni in a fixed-bed reactor, and success was achieved in reducing S species concentrations from 10 ppmv to 20 ppbv. The sulfur capacity varied from 2,000 to 10,000 ppmw or 0.2 to 1.0% by weight, depending on reactor conditions.

Initial work on sorbents containing dispersed Ni in an alumina (Al_2O_3) matrix was carried out by Swisher and Schwerdtfeger[16]. Two compositions were studied. One contained 26 wt % Ni in Al_2O_3, and the other contained 24 wt % Ni plus 7 wt % copper (Cu) in Al_2O_3. Copper was added because it is known to decrease the melting temperature and broaden the composition range of the liquid sulfide formed during sulfur sorption. There is a ternary eutectic reaction in the Ni-Cu-S system at 575°C. The eutectic composition in wt % is 69.8% Ni, 5.7% Cu, and 24.5% S[17,18]. The reactivity of individual pellets was studied in a Cahn thermogravimetric analyzer (TGA). Sulfidation was carried out in a mixture of 1 volume % H_2S in H_2, and regeneration was carried out in H_2. Results of the TGA experiments showed that the sorbents could be subjected to four sulfidation/regeneration cycles with no loss of reactivity. The temperature range for the experiments was 500° to 1000°C. It was found through visual observation and scanning electron microscopy that the liquid sulfide was retained in the Al_2O_3 structure during these TGA experiments.

PROJECT DESCRIPTION

Sorbent Preparation

The sorbent was prepared for evaluation using traditional powder processing methods. Reagent-grade NiO, CuO, and Al_2O_3 powders (all -325 mesh size) were blended in a 1 wt % solution of starch in water. Excess water was decanted, and the resulting paste was extruded through a metal tube to produce cylindrical pellets 9.3 mm in diameter and 10 to 12 mm long. The extrudates were dried in an oven at 120°C for 24 h. The dried extrudates were then placed in an electrically heated kiln; the temperature of the kiln was ramped up over a period of several hours, with a holding time of 2 h at the final sintering temperature of 1520°C. The extrudates were crushed and sieved to obtain samples in the -6, +16 mesh size range for fixed bed testing. The sorbent designation was 24Ni-7Cu-Al_2O_3, indicating a nominal composition of 24 wt % nickel and 7 wt % copper.

Description of Experimental Unit

The experimental studies were carried out in a bench-scale fixed bed reactor. A simplified schematic of the reactor system is shown in Figure 1. The reactor tube was alonized 316 stainless steel with an inside diameter of 2.21 cm (0.87 in) and a 0.165-cm (0.065-in) wall thickness. The sorbent bed was located in approximately the center of the 114.3-cm (45-in) long reactor tube, and the bed height was 5.08 cm

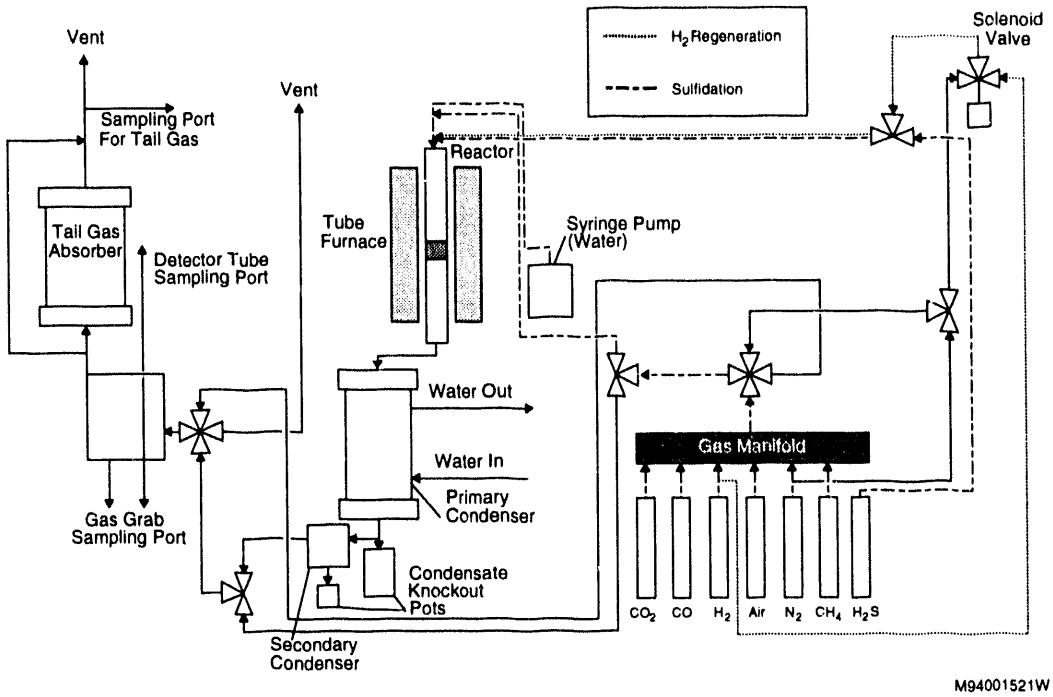

Figure 1. One-Inch Sorbent Screening Unit

(2 in). Gases were supplied from gas cylinders, and the flow rates were controlled through MKS mass flow controllers. All of the gases except hydrogen sulfide were first mixed together in a manifold prior to being fed into the reactor. Hydrogen sulfide gas was added to the other gases separately just upstream of the reactor inlet. Steam was provided by adding a predetermined amount of water into the preheated gas stream via an Isco model 100DM syringe pump. Both sulfidation and regeneration were conducted in the downflow mode. A heavy metal shield and a hydrogen flame detector with automatic reactive gas shutoff were installed for the protection of the operators from possible flames or explosions due to hydrogen leaks. The reactor temperature was maintained with a single-zone tubular electric furnace. The temperatures of the gases flowing into the bed and at the core of the bed (3.8 cm [1.5 in] from the bottom of the bed) were measured using type K thermocouples. The maximum allowable temperature of the reactor was 927°C (1700°F), which precluded doing the regeneration at higher and possibly kinetically more favorable temperatures. A preheat coil consisting of a 0.635-cm (0.25-in) outside diameter, 0.089-cm (0.035-in) wall thickness 316 stainless steel tube placed between the reactor and the furnace was used to preheat all inlet components, except for hydrogen sulfide and water, during the first two and a half cycles of sulfidation/regeneration. (A cycle is defined as one complete sulfidation followed by a complete regeneration of the sorbent.) This preheat coil was removed, and gases were heated to the required temperatures while passing through the top portion of the reactor tube during all subsequent experiments.

Experimental Procedure

Before the first sulfidation could be performed, the sorbent was pretreated to reduce the NiO to Ni metal. A 3-hour pretreatment with pure hydrogen was conducted at 871°C (1600°F) at the beginning of each series of cycles. A simulated Shell oxygen-blown entrained gasifier mixture was used as the sulfidation gas, and pure hydrogen was used as the regeneration gas. The Shell gas was chosen because it is the most likely to be applicable to this sorbent; clean fuel gas of this type could potentially be used instead of hydrogen for regeneration. The inlet gas compositions and other reaction conditions for sulfidation and regeneration are given in Table 1. Each sulfidation of the sorbent was stopped when the outlet concentration of H_2S reached 1000 ppmv. The regenerations were stopped when the outlet concentration of H_2S was less than or equal to 200 ppmv. The outlet stream was tested for hydrogen sulfide by the use of Sensidyne gas detector tubes of various ranges and gas grab samples, which were analyzed using gas chromatography.

A first series of six and a half cycles (designated JS1 experiments) were performed on the sorbent; afterward, the sorbent was removed from the reactor and sent for analysis. Blank runs on the empty reactor were conducted before and after the six and a half cycles of JS1 were performed; the blank runs consisted of two complete cycles of sulfidation/regeneration in each case. The reactor tube was replaced, and a second series of cycles were performed. The second series consisted of three and a half cycles (designated JS2 experiments). Two complete cycles of blank runs were conducted on the empty reactor just prior to performing the JS2 experiments.

The main difference between the JS1 and the JS2 series was that a preheat coil was located upstream of the reactor for the first two and a half cycles of the JS1 series. However, the preheat coil was removed after two and a half cycles and not replaced during the remaining experiments. The reason for removing it was that extensive carbon deposition in it caused a significant increase in pressure drop. It was thought that the carbon deposition occurred because, although the unalonized preheat coil had been passivated with nitric acid, it catalyzed the reaction in which carbon monoxide disproportionated to form carbon dioxide and carbon solids.

RESULTS

The H_2S breakthrough curves for the JS1 and JS2 series experiments are shown in Figures 2 and 3, respectively. It appears that the sorbent increased in capacity with each successive cycle, as evidenced by the longer times required for breakthrough. (Breakthrough is defined here as the point at which the concentration of H_2S in the outlet gas reaches 200 ppmv.) After the first three cycles of series JS1, and the first two cycles of JS2, the prebreakthrough concentration of H_2S in the outlet gas plateaued between 50 and 100 ppmv, with a gradual drift above these values as the sorbent approached breakthrough.

Since pure hydrogen was used as the regeneration gas, H_2S was released during regeneration. The regeneration curves showing H_2S outlet concentration as a function of time on-stream are shown in Figures 4 and 5 for the JS1 and JS2 series experiments, respectively. Note that the time required for regeneration increased during the first three cycles and then tended to stabilize. Regeneration took significantly more time than the corresponding sulfidation of the same cycle. Typically, the duration of each regeneration was more than six times that of the previous sulfidation.

Table 1. Reaction Conditions

Regeneration	Sulfidation
871°C (1600°F)	704°C (1300°F)
205 kPa (15 psig)	205 kPa (15 psig)
320 cc/min or 1000 1/hr	639 cc/min or 2000 1/hr
Regeneration Gas	Gas Mixture (Volume %)
Hydrogen 100.0%	Carbon Monoxide 64.1
End at 200 ppmv H_2S in Outlet	Hydrogen Sulfide 0.3
	Nitrogen 4.3
	Hydrogen 27.3
	Water 2.0
	Carbon Dioxide 2.0
	End at 1000 ppmv H_2S in Outlet

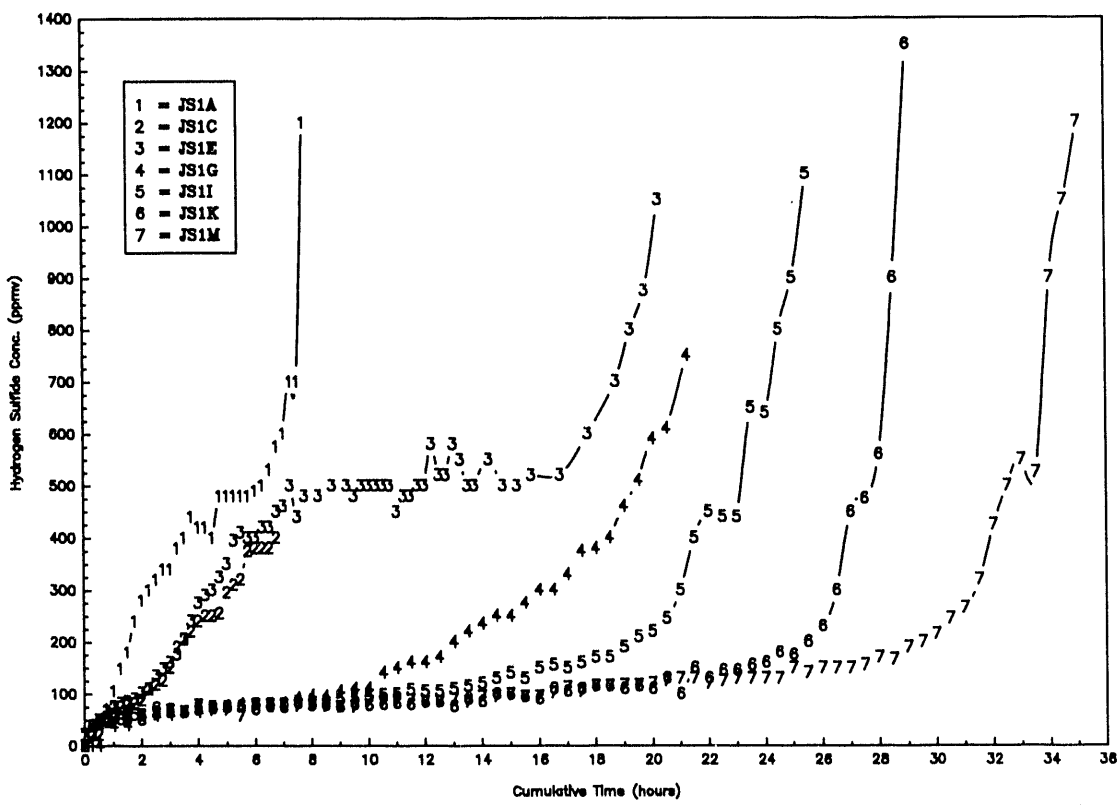

Figure 2. JS1 Sulfidation of 24Ni - 7Cu - Al_2O_3 at 704°C (1300°F)

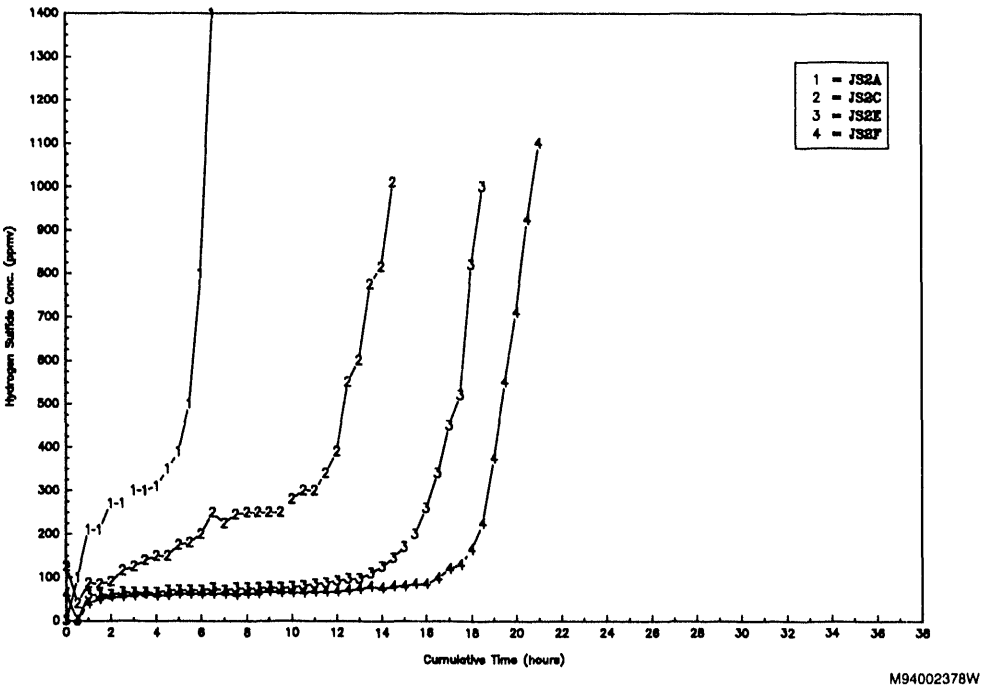

Figure 3. JS2 Sulfidation of 24Ni - 7Cu - Al_2O_3 at 704°C (1300°F)

Fig. 4 JS1 Regeneration of 24Ni - 7Cu - Al_2O_3 at 871°C (1600°F)

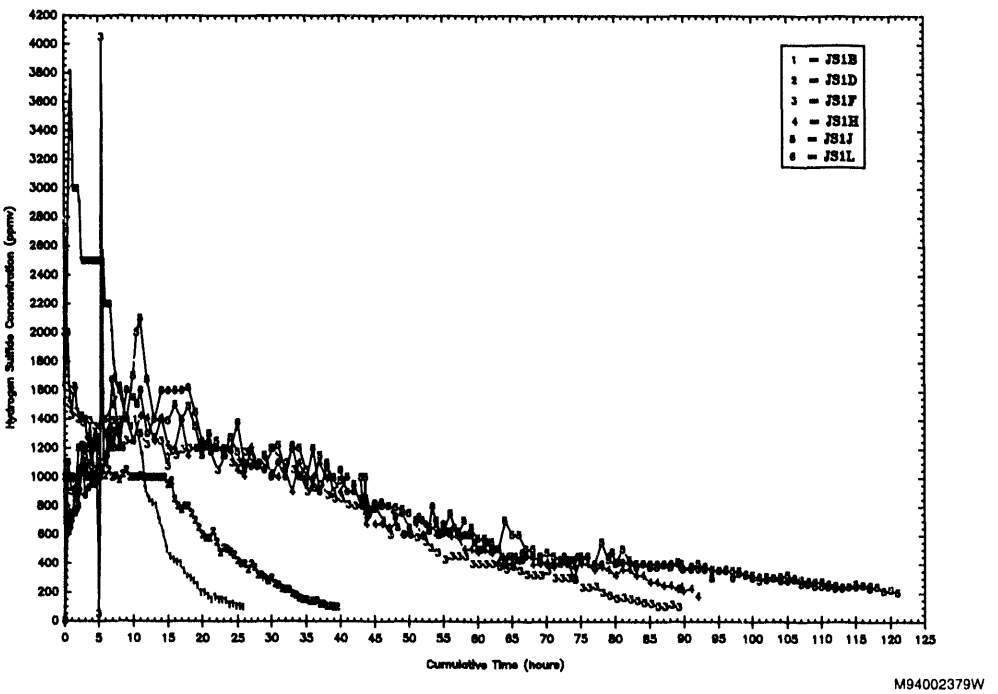

Figure 4. JS1 Regeneration of 24Ni - 7Cu - Al_2O_3 at 871°C (1600°F)

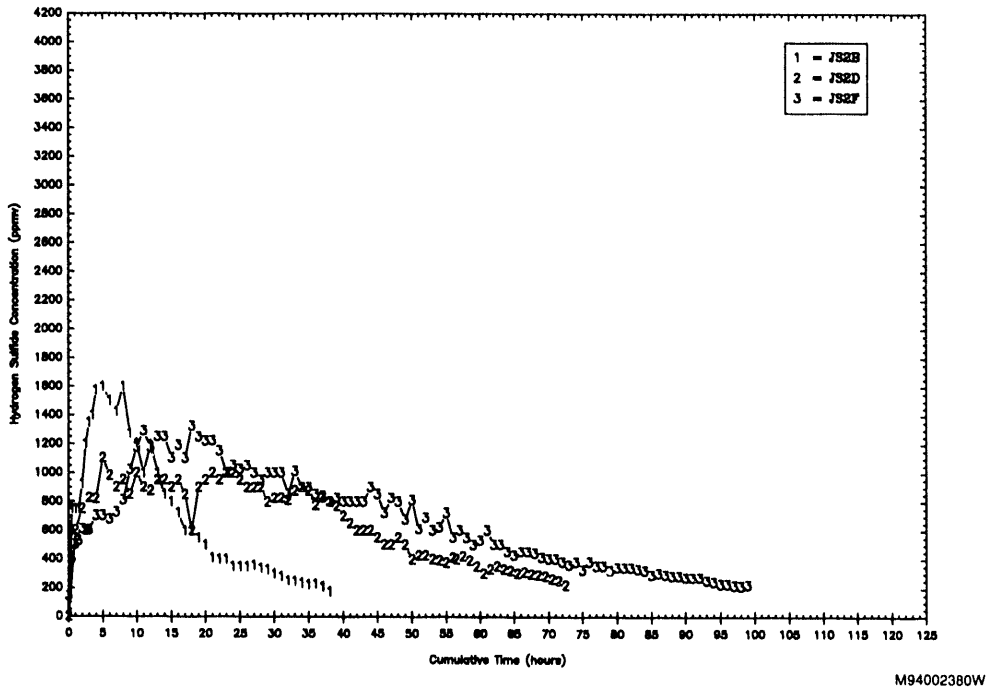

Figure 5. JS2 Regeneration of 24Ni - 7Cu - Al_2O_3 at 871°C (1600°F)

Figure 6 shows the H_2S breakthrough curves for the blank runs (empty reactor tests), which were conducted before and after the JS1 experiments and on the new reactor before the JS2 experiments. Breakthrough time on the empty reactor was significantly longer for runs conducted at the end of the test than those conducted at the beginning. However, the blank runs conducted at the end of the JS1 series had a much shorter breakthrough time than the 7th sulfidation, which was performed just prior to these, indicating that the sorbent had indeed increased remarkably in capacity.

Both the H_2S breakthrough curves and the regeneration curves shown in Figures 2 through 6 were determined using Sensidyne detector tubes. Gas chromatographic analysis of the reactor outlet gas, collected downstream from the condenser units during sulfidations, showed the dry basis volume concentrations of all the major gaseous components, in addition to H_2S, SO_2, and COS. Small amounts of methane (CH_4) were formed, resulting in a concentration that was always less than 0.8%. The SO_2 concentration usually stayed below 5 ppmv, with a few excursions to higher values during some of the sulfidations, after several hours on-stream. The concentrations of CO, CO_2, and H_2 indicated that little, if any, water-gas shift occurred. The COS concentration usually remained below 100 ppmv, and tended to increase during each experiment, as H_2S increased toward breakthrough.

The chemical compositions of the fresh sorbent and the sorbent reacted for six and a half cycles (JS1 series) are shown in Table 2. The atomic absorption analysis was run twice on both the fresh and spent sorbents to recheck the

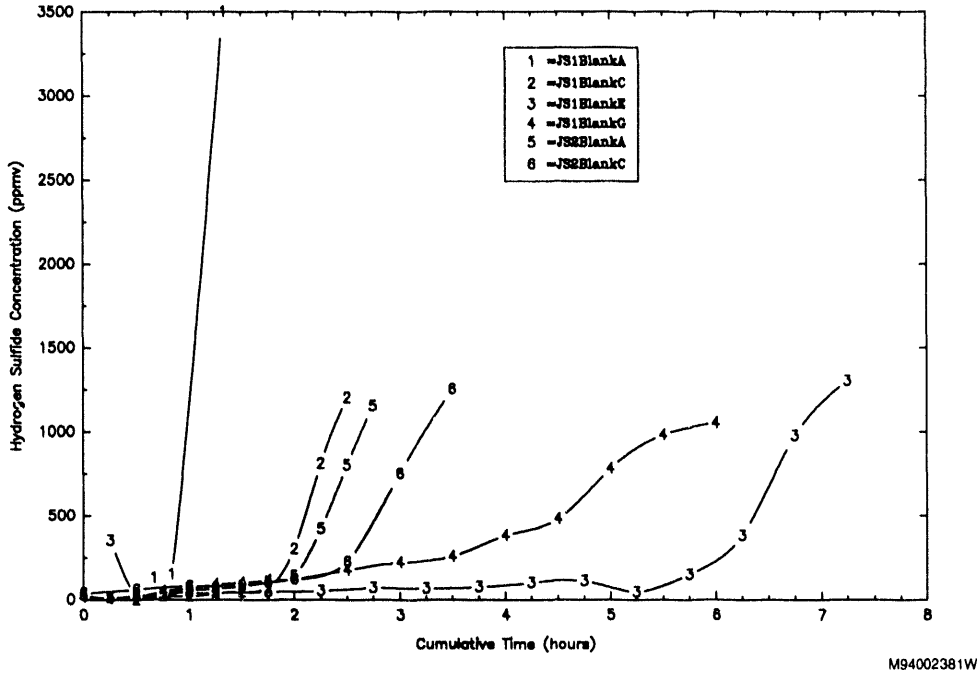

Figure 6. Blank Runs of 24Ni - 7Cu - Al_2O_3 at 704°C (1300°F)

Table 2. Chemical Compositions of Fresh and Reacted Sorbent

Element	Fresh (wt %)	Reacted (wt %)
Aluminum	28.10	28.60
Nickel	23.60	15.80
Copper	3.75	3.90
Total Sulfur	0.08	6.63

Ni content, resulting in exactly the same results for each. The analysis of Ni in the fresh sorbent also agreed quite well with the amount of Ni that was put into the sorbent during preparation (i.e., 24.0 wt % Ni was added during preparation, and the analysis showed 23.6 wt % Ni).

Calculations from the atomic absorption analysis of Al, Ni, and Cu were made assuming that the total amount of Al in the sorbent remained constant during the six and a half cycles. The calculations showed a 32% loss of Ni after the six and a half cycles; however, there was no loss of Cu. The sulfided sorbent contained 6.63 wt % sulfur. If it is assumed that each three Ni atoms can react with two S atoms to form Ni_3S_2 (although there are many different stoichiometric forms of Ni_xS_y possible[1]), and two Cu atoms react with one S atom to form Cu_2S, then the theoretical capacity of the sorbent is 9.54 g S/100 g fresh sorbent. Assuming the Al content of the sorbent to be constant, the actual sulfur content of the sorbent was 6.75 g S/100 g fresh sorbent, or 70.7% of theoretical capacity.

It should be noted that there is some question as to how the breakthrough time increased with each cycle, while there was simultaneously a loss of Ni from the sorbent. For example, fairly extensive redistribution of the remaining Ni would have to take place during hydrogen regeneration to compensate for this apparent volatilization loss of Ni.

Table 3 shows the physical characteristics of the fresh sorbent and the sorbent reacted for six and a half cycles (JS1 series). The mercury skeletal density, particle density, and cumulative pore volume remained essentially constant. However, the nitrogen pore volume increased seven-fold, and the BET nitrogen surface area increased 33-fold. The average pore diameter decreased to 28 percent of its original value. Porosity increased very little, if at all.

Electron micrographs of cross sections of the fresh and JS1 reacted sorbents are shown in Figure 7(a) and Figure 7(b), respectively. The sorbent appeared to be more uniform and more dispersed after reaction for six and a half cycles.

There was a concern about the possibility that some hydrogen embrittlement of the stainless steel reactor may have occurred, particularly during regeneration. Hydrogen embrittlement occurs when H_2 diffuses into the metal lattice and reacts with C in the metal to form CH_4. Cracks are formed as the CH_4 escapes. To determine whether this may have occurred, the reactor used during the JS1 series experiments was cut open length-wise, and electron micrographs were taken of the inner reactor wall. Microcracks and pitting were indeed observed on this inner surface of the reactor wall.

DISCUSSION

The 24Ni-7Cu-Al_2O_3 sorbent was unusual, compared to zinc-based and other sorbents, in that it increased in capacity with each successive cycle. The breakthrough curve performance of most sorbents tend to either stabilize after about three cycles, or gradually deteriorate with successive cycles. The physical characteristics of the fresh and reacted sorbent indicate that there was a large increase in surface area and in the number of small pores. This may have occurred through redistribution of the Ni and Cu to finer dispersions during each hydrogen regeneration.

The blank runs conducted on the empty reactor before and after the JS1 series experiments showed that there was increased sulfur sorption by the apparatus. Two possible explanations follow. Since there was an apparent large loss of Ni through volatilization from the sorbent, Ni may have been deposited on the walls of the reactor or downstream tubing, where it might have reacted with H_2S, resulting in a longer breakthrough time for the empty reactor. Electron micrographs suggested that hydrogen embrittlement of the reactor walls may also have occurred, resulting in microcracks which could penetrate the alonized surface, creating additional surface area for S sorption. However, it should be noted that the increase in breakthrough time on the empty reactor was small compared to the increase in breakthrough time between the first and seventh sulfidations. Therefore, the largest part of the increase in apparent sorbent capacity was due to changes in the sorbent itself. Corrective actions for the problem of hydrogen embrittlement could include the use of a reactor made of ceramic material, quartz, or an alloy with a very low C content.

Table 3. Physical Characteristics of Fresh and Reacted Sorbent

Item	Fresh	Reacted
N_2 Pore Volume (cc/g)	0.006354	0.04684
Hg Skeletal Density (g/ml)	4.16	4.20
Hg Bulk Density (g/ml)	2.38	2.37
Cum. Hg Pore Vol. (ml/g)	0.18	0.19
Surface Area (m^2/g)	0.0963	3.21
Avg. Pore Diameter (μm)	0.5858	0.1622
Porosity (%)	42.79	43.76

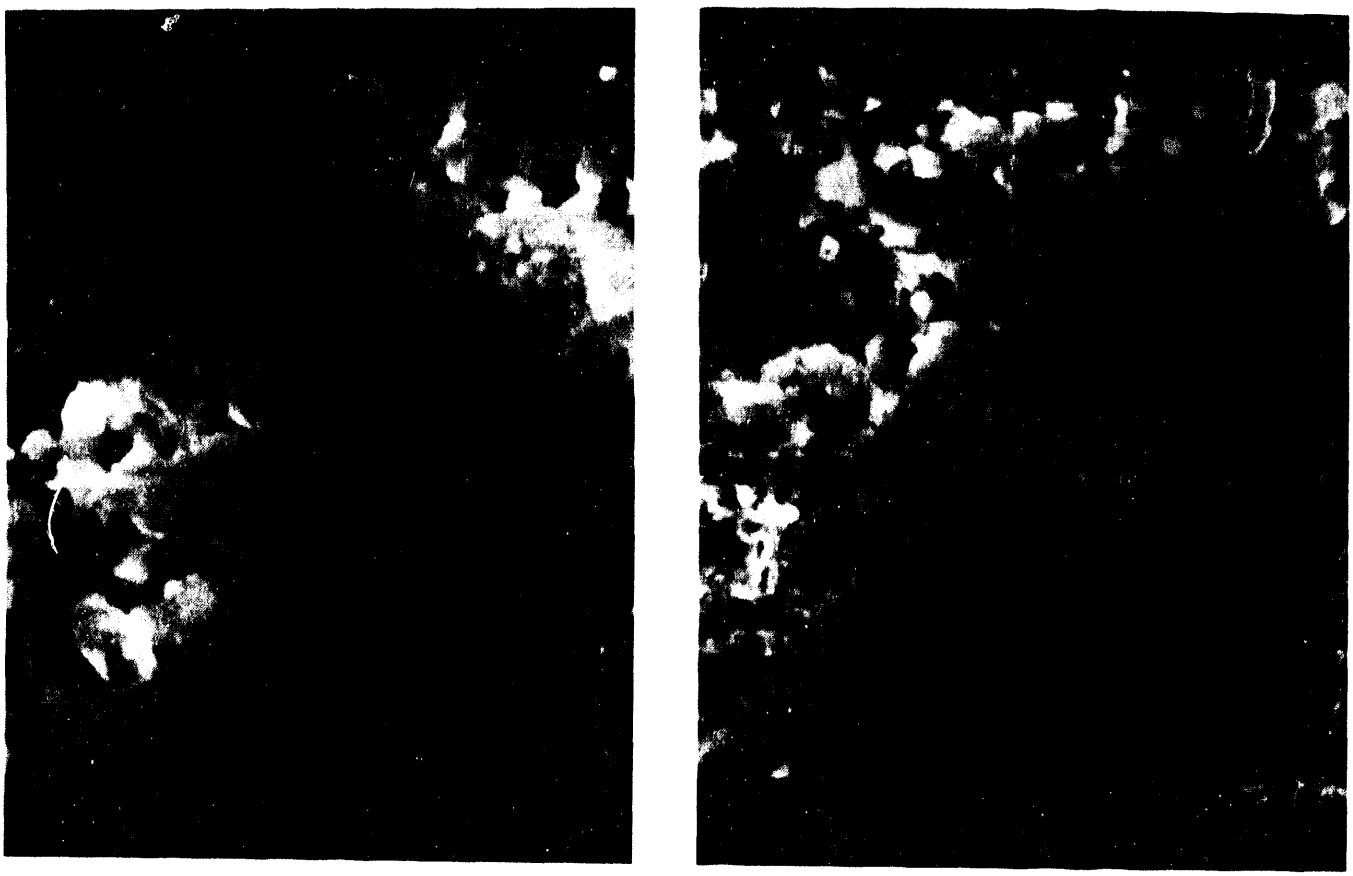

7a. Fresh **7b. After Six and a Half Cycles**

Figure 7. 24 Ni - 7Cu - Al_2O_3 Sorbent Magnified 3,000 Times

The prebreakthrough concentration of H_2S in the outlet gas was higher than expected. Patel, Rich, and Maru[15] had observed a reduction in S species concentration from 10 ppmv to 20 ppbv; in that case, a typical commercial Ni catalyst, 20 wt % Ni on Al_2O_3, was used for H_2S removal from a simulated coal gas. However, in the present study, the higher levels of inlet H_2S concentration apparently caused the reactive surface sites to become rapidly occupied by sulfur, after which bulk sulfidation took place.

Sulfides that form in commonly studied sorbents, such as zinc ferrite and zinc titanate, are solids at their hot gas desulfurization reaction temperatures. However, nickel sulfide became a liquid at the reaction conditions studied here. Since liquids tend to have higher vapor pressures than solids, it might be expected that the liquid nickel sulfide could give rise to vapors which could then be swept away by the simulated coal gas.

Long regeneration times were required by the sorbent (usually at least six times as long as the respective sulfidation breakthrough time, and as much as 22 times longer). If it is assumed that the species to be regenerated were Ni_3S_2 and Cu_2S, 70.7% of theoretical capacity of the sorbent had been reached (9.54 g sulfur/100 g fresh sorbent), and the shortest regeneration time observed is considered (i.e., from the first cycle of the JS1 series), then 310 gmoles of H_2 were required to remove each gmole of S from the sorbent. This makes the sorbent impractical for commercial use in a fixed-bed mode under these conditions, since at least as many reactors as the greatest number of times the length of regeneration was greater than its respective sulfidation would be required. Also, large volumes of reducing gas would be required for regeneration. However, it should be noted that Jhunjhunwala[1] showed in TGA experiments that when sulfidation was carried out at 700°C and regeneration at 950°C on the same type of sorbent, the regeneration time was slightly less than the time required for sulfidation. Unfortunately, the fixed-bed unit used in the present studies could not be operated at temperatures greater than 871°C.

FUTURE WORK

Since the presence of copper tends to reduce the temperature at which liquid nickel sulfides form, a Ni/Al_2O_3 without copper will be studied. Also, a lower reaction temperature will be used (593°C [1100°F] instead of 704°C [1300°F]); hopefully, this will help avoid nickel loss through volatilization. Since the time required for hydrogen regeneration was unacceptably long, oxidative regeneration will be attempted and directly compared with hydrogen regeneration.

ACKNOWLEDGMENTS

The authors would like to gratefully acknowledge the work performed by the METC operators of the bench-scale, fixed-bed reactor, which was used for these studies. Many 12-hour shifts were conducted by Lanny Golden, Todd Gardner, Ed Fisher, Grover Evans, Gary McDaniel, and Karl Warnick to make collection of this data possible.

This research was supported in part by an appointment to the U.S. Department of Energy Fossil Energy Postgraduate Research Training Program, administered by the Oak Ridge Institute for Science and Education.

REFERENCES

1. Jhunjhunwala, M., "Evaluation of Dispersed Nickel Sorbents for Hot Gas Desulfurization," Masters Thesis, Department of Mechanical Engineering and Energy Processes, Southern Illinois University at Carbondale, July, 1993.

2. Swisher, J. H., and Schwerdtfeger, K., "Review of Metals and Binary Oxides as Sorbents for Removing Sulfur from Coal-Derived Gases," *J. Mat. Eng. and Perf.*, *1*(3), 1992, 399-407.

3. Swisher, J. H., and Schwerdtfeger, K., "Thermodynamic Analysis of Sorption Reactions for the Removal of Sulfur from Hot Gases," *J. Mat. Eng. and Perf.*, *1*(4), 1992, 565-571.

4. Grindley, T. and Steinfeld, G., "Development and Testing of Regenerable Hot Coal-Gas Desulfurization Sorbent," Report No. DOE/METC-16545-1125, Morgantown Energy Technology Center, Morgantown, WV, 1981.

5. Mei, J. S., Gasper-Galvin, L. D., Everitt, C. E., and Katta, S., "Fixed-Bed Testing of a Molybdenum-Promoted Zinc Titanate Sorbent for Hot Gas Desulfurization," *Proceedings of the Coal-Fired Power Systems 93--Advances in IGCC and PFBC Review Mtg.*, D. L. Bonk, ed., DOE/METC-93/6131, Springfield, Va.: National Technical Information Service, 1993, 315-325.

6. Ayala, R. E., Gal, E., and Gupta, R. P., "Testing of Zinc Titanate Desulfurization Sorbents for Moving Bed Applications," Ibid., 136-145.

7. Gangwal, S. K., and Gupta, R. P., "Enhanced Durability of Desulfurization Sorbents for Fluidized-Bed Application," Ibid., 146-157.

8. Swisher, J. H., "An Attrition-Resistant Zinc Titanate Sorbent for Sulfur," Final Technical Report submitted to the Illinois Clean Coal Institute, Carterville, Illinois, Sept. 1993.

9. Swisher, J. H., O'Brien, W. S., and Gupta, R. P., "An Attrition-Resistant Zinc Titanate Sorbent for Sulfur," Quarterly Technical Reports submitted to the Illinois Clean Coal Institute, Carterville, IL, Dec. 1993 and Mar. 1994.

10. Gupta, R. P., Gangwal, S. K., and Jain, S. C., "Fluidizable Zinc Titanate Materials with High Chemical Reactivity and Attrition Resistance," U. S. Patent No. 5,254,516, Awarded to Research Triangle Institute, Research Triangle Park, NC, 1993.

11. Nagamori, M., and Ingram, T. R., "Thermodynamic Properties of Ni-S Melts Between 700° and 1100°C," *Met. Trans.*, *1*, 1970, pp. 1821-1825.

12. Rosenquist, T., "A Thermodynamic Study of the Iron, Cobalt, and Nickel Sulphides," *J. Iron and Steel Inst.*, *175*, 1954, 37-57.

13. Elliott, R. P., *Constitution of Binary Alloys, First Supplement*, McGraw-Hill, New York, 1965, 669.

14. Steiner, P. and Gutterman, C., "Nickel Sulfide Method for Separating Hydrogen Sulfide," Foster Wheeler Energy Corp., Clinton, NJ, German Patent No. DE 29 03 377 Al, 1979 (in German).

15. Patel, P. S., Rich, S. M., and Maru, H. C., "Trace Contaminant Removal from Hot Coal Gas for Molten Carbonate Fuel Cell Applications," *Proceedings of the Fifth Annual Contractors Meeting on Contaminant Control in Coal-Derived Gas Streams*, D. C. Cicero and K. E. Markel, eds., DOE/METC-85/6025, Springfield, Va.: National Technical Information Service, 1986, 419-424.

16. Swisher, J. H., and Schwerdtfeger, K., "The Behavior of Sulfur Sorbents Containing Dispersed Nickel," *Proc. 9th Annual Int. Pittsburgh Coal Conf.*, 1991, 646-653, Available from Conference Services, P.O. Box 270, Greensburg, Pennsylvania 15601.

17. Boldt, J. R., *The Winning of Nickel*, Methuen and Co., Ltd., London, UK, 1967, 275-280.

18. Sproule, K., Harcourt, G. A., and Renzoni, L. S., "Treatment of Nickel-Copper Matte," in *Extractive Metallurgy of Copper, Nickel, and Cobalt*, P. Queneau, ed., Interscience Publ., New York, New York, 1961, 33-52.

LGASPE\1:940851

P3 Pilot Gasification and Hot Gas Cleanup Operations

John M. Rockey, Edwin Galloway, and Teresa A. Thomson
Morgantown Energy Technology Center

Jay Rutten and Alain Lui
EG&G Technical Services of West Virginia

ABSTRACT

The Morgantown Energy Technology Center (METC) has an integrated gasification hot gas cleanup facility to develop gasification, hot particulate and desulfurization process performance data for IGCC systems.

The objective of our program is to develop fluidized-bed process performance data for hot gas desulfurization and to further test promising sorbents from lab-scale screening studies at high-pressure (300 psia), and temperatures (1,200°F) using coal-derived fuel gases from a fluid-bed gasifier.

The 10-inch inside diameter (ID), nominal 80 lb/hr, air blown gasifier is capable of providing about 300 lb/hr of low BTU gas at 1,000°F and 425 psig to downstream cleanup devices. The system includes several particle removal stages, which provide the capability to tailor the particle loading to the cleanup section.

The cleanup test section consists of a closely coupled modular gas cleanup rig (MGCR) which was acquired from The Institute of Gas Technology.

The MGCR receives coal-derived gas at 425 psig and 1,000°F from the METC Fluid-Bed Gasifier. The gas pressure is reduced to approximately 300 psia and filtered by a candle filter vessel containing up to four filter cartridges. For batch-mode desulfurization test operations, the filtered coal gas is fed to a 6-inch ID, fluid-bed reactor that is preloaded with desulfurization sorbent.

Over 400 hours of gasifier operation was logged in 1993 including 384 hours of integration with the cleanup rig. System baseline studies without desulfurization sorbent and repeatability checks with zinc ferrite sorbent were conducted before testing with the then most advanced zinc titanate sorbents, ZT-002 and ZR-005.

In addition to the desulfurization testing, candle filters were tested for the duration of the 384 hours of integrated operation. One filter was taken out of service after 254 hours of filtering while another was left in service. At the conclusion of testing this year it is expected that 3 candles, one each with 254, 530, and 784 hours of filtering will be available for analysis for effects of the exposure to the coal gas environment.

P4

Coal Ash Behavior in Reducing Environments

CONTRACT INFORMATION

Contract Number DE-FC21-86MC10637

Contractor

Energy & Environmental Research Center
University of North Dakota
PO Box 9018
Grand Forks, ND 58202-9018
(701) 777-5000

Contract Project Manager Steven A. Benson

Principal Investigators

Thomas A. Erickson
David W. Brekke
Bruce C. Folkedahl
James E. Tibbetts
Jan W. Nowok

METC Project Manager Venkat K. Venkatarman

Period of Performance November 1, 1990, to October 31, 1994

Schedule and Milestones

FY94 Program Schedule

	N	D	J	F	M	A	M	J	J	A	S	O
Task 1												
Task 2												
Task 3												

OBJECTIVES

The objective of the Coal Ash Behavior in Reducing Environments (CABRE) program is to advance the knowledge of ash behavior in coal gasification systems; this knowledge will help provide the understanding necessary to operate advanced coal utilization systems efficiently with a minimum of the operational problems associated with ash properties. The program approach is to use carefully controlled, laboratory-scale experiments coupled with detailed analysis of the materials involved to determine the critical fundamental mechanisms of ash behavior in coal gasification systems.

BACKGROUND INFORMATION

A key factor in the successful design and operation of coal gasification systems is the ability to control and mitigate ash-related problems. Some of the major ash-related problems are slag flow control, slag attack on the refractory, ash deposition on heat-transfer surfaces, corrosion and erosion of equipment and materials, and emissions control. Such problems are closely tied to the abundance and association of inorganic components in coal and gasification conditions.

In general, the inorganic components are associated in the coal as minerals or organic complexes (salts of carboxylic acid groups or organic coordination complexes). The minerals associated in coal vary widely in size, composition, and juxtaposition. Juxtaposition refers to the association of mineral grains with other mineral grains and coal particles. These associations directly influence the chemical and physical transformations that occur during the gasification process. Depending upon the type of gasification system, inorganic components are initially partitioned into intermediate species in the form of inorganic gases, liquids, and solids. The state of these species at any given stage or position in the gasifier directly influences their behavior at that stage. The transformations and partitioning of inorganic species directly influence slag behavior, extent and type of slag attack on the refractory, and corrosion and erosion of materials, as well as growth rate, quantity, and type of ash deposition on heat-transfer surfaces.

PROJECT DESCRIPTION

The CABRE project is a four-year program designed to investigate the transformations and properties of coal ash in reducing environment systems. This project is currently midway through its third year. The work to date has emphasized four areas of research: 1) the development of quantitative techniques to analyze reduced species, 2) the production of gasification-type samples under closely controlled conditions, 3) the systematic gasification of specific coals to produce information about their partitioning during gasification, and 4) the study of the physical properties of ashes and slags under reducing atmospheres.

The CABRE project is organized into three tasks which provide a strong foundation for the project. Task 1, Analytical Methods Development, has concentrated on the special needs of analyzing samples produced under a reducing atmosphere as opposed to the more often studied combustion systems. Task 2, Inorganic Partitioning and Ash Deposition, has focused on the production of gasification-type samples under closely controlled conditions for the study of inorganic partitioning that may lead to deposition. Task 3, Ash and Slag Physical Properties, has made large gains in the areas of sintering and strength development of coal ashes under reducing atmospheres for the evaluation of deposition problems.

RESULTS

Task 1 - Analytical Methods Development

The scanning electron microscope (SEM) technique most commonly used at the Energy & Environmental Research Center (EERC) to characterize deposits is the scanning electron microscopy point count (SEMPC) technique (Steadman and others, 1990), Figure 1. This technique was developed at the EERC to

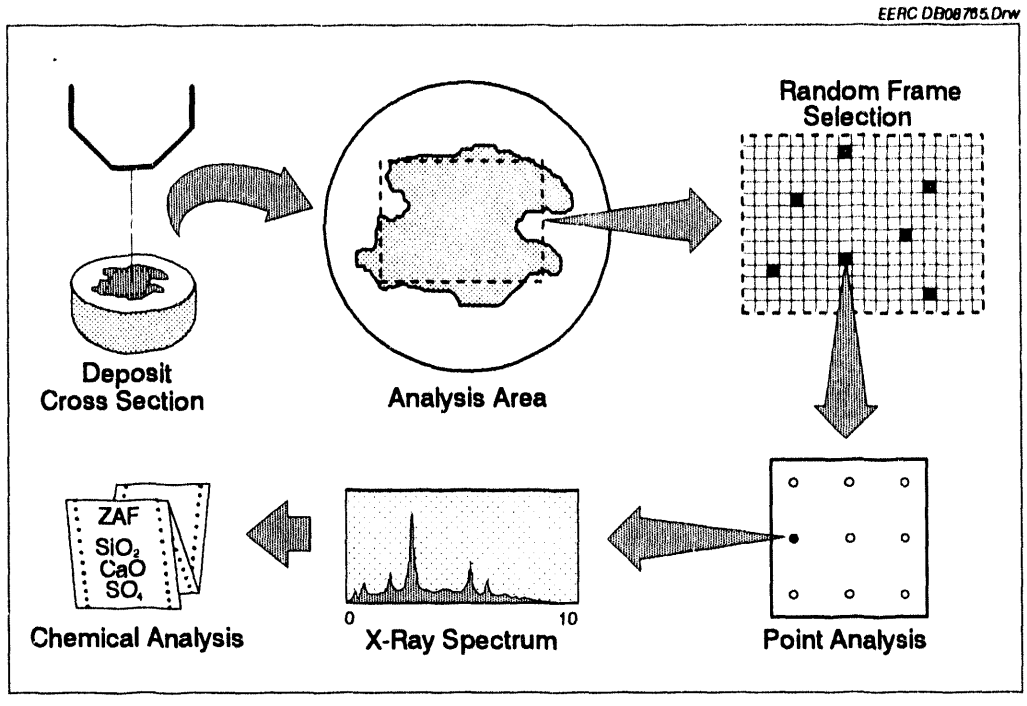

Figure 1. Scanning Electron Microscope Point Count Analysis Routine

quantitatively determine the relative amounts of the phases present in entrained ashes and deposits. The method involves microprobe analysis (for chemical compositions) of a large number of random points on a polished cross section of a sample. A data manipulation program then classifies each chemical composition into a phase category based on various weight and molar ratios. The criteria for the classification procedure have been developed from the stoichiometry of the various phases.

The most important addition to this technique from the CABRE project was the qualitative examination of carbon and oxygen during analysis. Carbon and oxygen are two of the more important chemical components in reducing environments. A rapid and accurate analysis of these elements concurrent with the analyses of other elements in an energy-dispersive x-ray spectrometer system is very advantageous. However, due to the complexity of the samples analyzed in this project, problems arise which hinder the quantification of carbon and oxygen. The samples vary widely in composition and, therefore, do not present a consistent background matrix to the correction routines. All samples must be carbon-coated to maintain conductivity under the electron beam. The best result that can be attained under these conditions is a qualitative/semiquantitative determination of carbon and oxygen. The advances made concerning carbon and oxygen determinations have been previously documented (Erickson and Others, 1993)

In conjunction with the SEMPC technique, three data manipulation programs were created to manipulate the data and present them in their best format: MINCLASS© for Microsoft® MS-DOS® (DOS), MINCLASS© for Microsoft® Windows™ (Windows), and VISCALC© for DOS. Each of these codes are discussed below.

MINCLASS©

The phase classification program, MINCLASS© 4.0, has been revised to incorporate advances in hardware and increased knowledge about the analytical demands of the CABRE project. Improvements include modifying the classification algorithms to incorporate quantified oxygen values, which allows any element to be included in the analysis, and tabulating the number of points that make up the various chemical composition summaries. These refinements make it easier to analyze SEMPC data from reducing environment samples where reduced phases are difficult to recognize.

A Windows version of MINCLASS© was also made available to those desiring to operate in that environment. This version of the program requires Windows 3.1 as the operating environment. The input file, classification routine, and output files are the same as the DOS version. Either program will produce the same results. Included in the MINCLASS© for Windows interface is the viscosity calculation program VISCALC©. An example of the output from MINCLASS© 4.0 is given in Table 1.

VISCALC©

A silicate liquid-phase viscosity calculation and viscosity distribution program named VISCALC© 4.0 is available to sponsors for the first time. VISCALC© has been used internally on CABRE samples since the beginning of the project. The program uses the chemistry and mineralogy of silicate and aluminosilicate phases determined by the SEMPC technique. Mineralogy is used to determine which phases to include in the viscosity calculations. Chemistry is used as input to a model developed by Kalmanovitch and Frank (1988) to calculate viscosity. The model is based on a modified version of a metallurgical slag viscosity model developed by Urbain and others (1981). Assumptions in the model include the chemistry expressed as oxides, iron expressed in the ferric state, and calculations performed only on silicate and aluminosilicate phases.

In addition to a file of calculated viscosities, the program includes an interactive graphics feature for comparing viscosities. The present version of VISCALC© allows the user to compare the viscosities of a single sample as three temperatures or up to three different samples at a single temperature. If certain silicate phases are known to be crystalline at the input temperatures, VISCALC© permits them to be excluded from the viscosity calculations. It is up to the user to decide which phases are to be excluded. An example of the output from VISCALC© is given in Table 2.

Task 2 - Inorganic Partitioning and Ash Deposition

The production of gasification-type samples under closely controlled conditions has been the primary goal of Task 2 for the duration of this project. A pressurized drop-tube furnace (PDTF) is used to produce the gasification samples. The PDTF can closely control the temperature profile, pressure, atmosphere, and residence time. The use of a small-scale gasifier such as this allows for the fundamental research of coal gasification without a large capital investment for equipment.

Table 1. Example Output from MINCLASS© Software

UND-EERC SEMPC Mineral Classification Version 3.1
Run Date: December 17, 1992, Using Definitions File rules. c

Mineral Name	Frequency Percent	Mineral Name	Frequency Percent
Oxide-Rich		Silicon-Rich	
Magnesium Oxide	0.0	Quartz	25.1
Aluminum Oxide	0.0	Albite	0.3
Calcium Oxide	0.0	Anorthite	0.0
Titanium Oxide	0.0	Potassium Feldspar	0.0
Chromium Oxide	0.0	Nepheline	0.0
Iron Oxide	0.3	Hauyne	0.0
Spinel	0.0	Leucite	0.0
Ca-Ti Oxide	0.0	Kaolinite	8.1
Ca-Al Oxide	0.0	Altered Kaolinite	2.7
Mixed Oxide-Rich	1.0	Illite	0.3
Total for Group	1.4	Montmorillonite	2.7
		Pyroxene	0.0
Sulfur-Rich		Wollastonite	0.0
Pyrite	0.0	Calcium Silicate	0.0
Pyrrhotite	0.0	Di Calcium Silicate	0.0
Iron Sulfate	0.0	$Na\text{-}Ca\text{-}SiO_3$	0.0
Sodium Sulfate	0.0	Gehlenite	0.0
Calcium Sulfate	0.7	Akermanite	0.0
Na-Ca Sulfate	0.0	Merwinite	0.0
Barite	0.3	Spurrite	0.0
Mixed Sulfur-Rich	0.0	Mullite	0.0
Total for Group	1.0	Mixed Silicon-Rich	0.2
		Total for Group	49.5
Phosphorous-Rich			
Apatite	0.0		
Mixed Phosphorous-Rich	0.0	User-Defined List	
Total for Group	0.0	Ettringite	0.3
		Calcium Aluminate	1.0
Carbon-Rich		Total for Group	1.4
Calcite	7.8		
Altered Calcite	0.0		
Dolomite	0.3		
Sulfated Dolomite	0.0	Other	9.5
Ankerite	0.0		
Sulfated Ankerite	0.0		
Mixed Carbon-Rich	8.8		
Total for Group	36.9		

Table 1 (continued)

Mineral Name	Frequency Percent	Mineral Name	Frequency Percent
Metal-Rich			
Aluminum	0.0		
Titanium	0.0		
Iron	0.0		
Nickel	0.0		
Copper	0.0		
Chromium	0.0		
Mixed Metal-Rich	0.3		
Total for Group	0.3		

Total Number of Points Analyzed = 295
Carbon Threshold for Analysis = 2000
Oxygen Threshold for Analysis = 300

Bulk Chemical Composition, oxide wt%

	A	B	C	D	E	F	G
SiO_2	4.9	1.6	62.2	1.5	48.2	55.5	56.0
Al_2O_3	19.5	26.8	20.1	37.4	15.0	17.4	17.9
Fe_2O_3	14.7	5.9	2.4	5.7	4.6	4.0	4.2
TiO_2	2.2	1.7	0.7	0.9	3.1	1.1	1.3
P_2O_5	0.1	0.0	0.2	0.0	0.1	0.1	0.1
CaO	41.5	30.9	5.1	48.7	17.2	12.7	13.4
MgO	13.2	3.9	2.6	5.0	4.2	3.5	3.6
Na_2O	1.9	0.5	4.2	0.4	5.9	3.2	3.3
K_2O	0.1	0.1	0.5	0.0	0.5	0.3	0.3
SO_3	0.5	3.6	0.4	0.3	0.2	0.8	0.0
Cl_2O_7	0.5	0.4	0.8	0.0	0.2	0.5	0.0
Cr_2O_3	0.1	0.0	0.1	0.0	0.1	0.1	0.0
BaO	0.7	24.6	0.6	0.0	0.7	0.9	0.0
Points	26	3	23	1	1	295	295

A Cumulative bulk composition of other.
B Cumulative bulk composition of mixed oxide-rich.
C Cumulative bulk composition of mixed carbon-rich.
D Cumulative bulk composition of mixed metal-rich.
E Cumulative bulk composition of mixed silicon-rich.
F Cumulative bulk composition of the entire sample.
G SO_3-, Cl_2O_7-, Cr_2O_3-, BaO-free composition of the entire sample.

Table 2. Example Output from VISCALC© Software

12345678 Test Sample
Viscosity Data

Index	1100.0	1300.0	1500.0	Temp. at 3.0 Critical Viscosity
1	4.065	2.868	1.948	1275.1
2	2.963	1.995	1.251	1093.6
3	3.606	2.505	1.658	1203.0
4	7.108	5.281	3.873	1652.1
5	3.810	2.666	1.786	1235.5
6	3.066	2.076	1.316	1111.6
7	3.118	2.117	1.349	1120.8
8	5.728	4.187	3.000	1500.1
9	5.578	4.068	2.905	1481.6
10	5.744	4.199	3.010	1501.8
11	3.670	2.555	1.698	1213.6
12	4.009	2.824	1.912	1266.7
13	4.015	2.828	1.916	1267.6
14	5.707	4.170	2.986	1497.4
15	5.839	4.275	3.070	1513.3
16	5.146	3.725	2.631	1427.1
17	5.530	4.030	2.875	1475.9
18	3.416	2.353	1.537	1171.8
19	3.710	2.587	1.723	1219.7
20	4.842	3.484	2.439	1386.7
21	6.153	4.524	3.269	1549.7
22	6.115	4.493	3.244	1545.3
23	10.084	7.640	5.755	1726.8
24	5.266	3.820	2.707	1442.5

Viscosity frequency distribution data:

0-1	1-2	2-3	3-4	4-5	5-6	6-7	7-8	8-9	9-10	10-11	11-12
1500											

Table 2 (continued)

Viscosity frequency distribution data:

0.0	45.8	25.0	25.0	0.0	4.2	0.0	0.0	0.0	0.0	0.0	0.0
1300											
0.0	4.2	41.7	12.5	33.3	4.2	0.0	4.2	0.0	0.0	0.0	0.0
1100											
0.0	0.0	4.2	29.2	16.7	33.3	8.3	4.2	0.0	0.0	4.2	0.0

T_{cv} cumulative % less than frequency data:

<70	80	90	100	110	120	130	140	150	160	170	180	190	>1900
0.0	0.0	0.0	0.0	4.2	16.7	45.8	50.0	70.8	91.7	95.8	100	100	100

The PDTF is a laboratory-scale, vertically oriented, downfired, entrained flow furnace able to perform gasification studies under closely controlled conditions. The PDTF furnace assembly, Figure 2, consists of an upper alumina tube (2.875-in. ID x 55 in. long) and a lower alumina tube (2.875-in. ID x 25 in. long) separated by a flow accelerator. The two vertically oriented tubes are held in position by a slightly larger concentric tube. The tube assembly is heated externally with three high-temperature tube furnaces (four heating zones) equipped with Kanthal Super 33 elements capable of heating the furnace to 1500°C. Each of the heating zones can be controlled separately for temperature profiling. The top two furnaces are used for the gasification zone, while the bottom furnace is used as a deposition and collection zone. The entire reactor, including the heating elements, is housed in a water-jacketed pressure vessel rated at 335 psi.

Fluidized coal, 80% −200 mesh, is introduced into the reactor with a carrier gas (primary gas) through a traversing, water-cooled injector positioned in the center of the tube. The feeding system allows close control of feed rates as low as 0.1 g/min. Optional (secondary) gas enters the reactor at the top of the tube and flows down through the tube around the injector assembly. The coal residue and process gases travel down the reactor tube in a laminar flow regime and pass through the accelerator where they are collected by a water-cooled, nitrogen-quenching ash collection probe or water-cooled deposition probe. Particle residence times can be controlled by inserting or retracting the coal injector into the furnace while the collection device remains fixed. Various collection devices can be attached to the outlet of the collection probe to collect the solids. Size segregation of the ash is facilitated by using a multicyclone or impactor in conjunction with a final filter. A bulk filter is used to collect ash for bulk

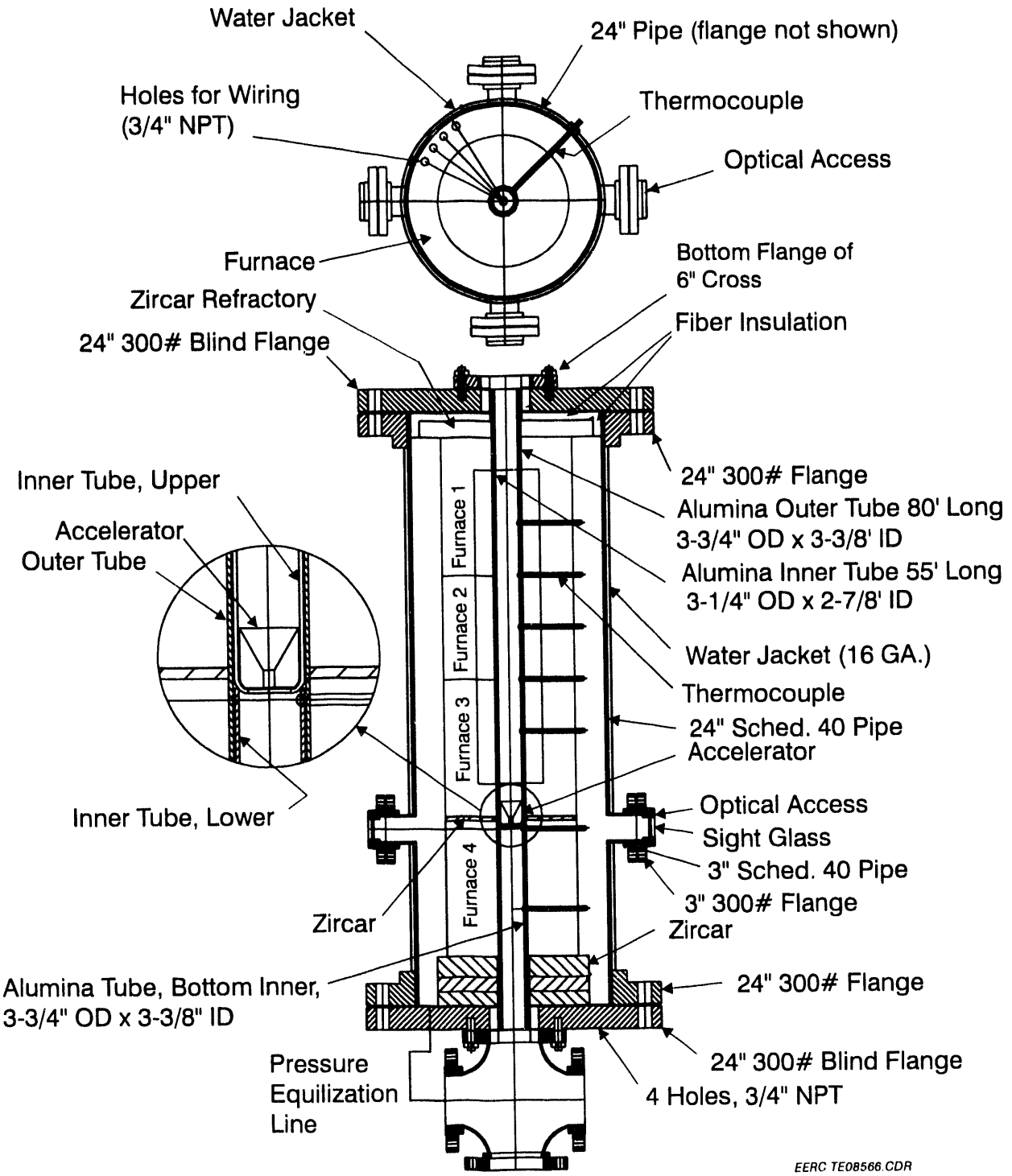

Figure 2. PDTF Assembly

chemistry. The process gases exiting the collection device are monitored on-line by O_2, CO, or CO_2 gas analyzers or off-line by a gas chromatograph (GC).

Deposition tests were conducted over the last twelve months on five coals: Sufco/Hiawatha, Illinois No. 6, Pittsburgh No. 8, Drayton, and Rochelle. These tests were conducted at a gasification temperature of 1500°C and deposition zone temperatures of 1000° and 800°C. The results from these tests are currently being investigated, and replicate runs are being performed for verification.

To enhance the work done in the PDTF, thermochemical equilibrium modeling was done to predict slag flow behavior. Thermochemical equilibrium modeling is an effective method to predict behavior in well-mixed equilibrium systems. Though slag in a gasifier is not an equilibrium mixture, it does approach equilibrium because of its high molten state. PHOEBE©, a thermochemical equilibrium code developed at the EERC, has been used extensively in the past to model high-temperature slags and deposits in combustion systems. With the latest enhancements to its database, it is now capable of modeling gasification systems as well. Three of the coals from the CABRE project have been run through the code at temperatures ranging from 1500° to 3000°F (815° to 1650°C). Both the viscosity and percent of ash as liquid phase were recorded for each temperature and coal.

The chemical compositions used in these predictions come from the original coal analysis (ultimate and x-ray flouresence). It should be noted that the composition of a slag in a real gasifier may be different because of the partitioning of specific species caused by the aerodynamic properties of the reactor. Figures 3-5 show the results of the modeling predictions. Each of the three graphs shows a temperature range at which there is no appreciable amount of liquid phase present, followed by an increase in the liquid phase amount and a decrease in its viscosity. The phases and their corresponding viscosities change as a function of temperature.

Task 3 - Ash and Slag Physical Properties

The third task of the CABRE project has concentrated on the various physical processes that take place in the formation of slags and deposits on various heat-exchange surfaces. The primary emphasis has been on the process of strength development under reducing conditions. The results of this project, along with literature on similar subjects, have pointed to the presence of three different strength development regimes (Figure 6) as defined by the dominant liquid phases: sulfides, sulfided silicates, and silicates. Figure 7 shows the thermal stability of various sulfides as determined under an atmosphere of $H_2S/CO_2/CO$.

Much of the work over the past year has focused on the effects of water vapor on the sintering potential of coal ashes. Three different sulfides were tested in a thermogravimetric analyzer (TGA) with and without the presence of water vapor. The results for $Fe_{1-x}S$, CaS, and Na_2S-1.7FeS are shown in Figures 8, 9, and 10, respectively. The iron sulfide appears to be relatively unaffected by the presence of the water vapor. The stability of the calcium sulfide is shifted to lower temperatures by the presence of water vapor. The Na_2S-1.7FeS system appears to undergo a more complex interaction with the water vapor which

involves the addition of weight to the system. It is possible that some of the sodium sulfide is being replaced with NaOH, which would involve a slight increase in weight.

FUTURE WORK

Over the final half year, the CABRE project will continue to study the transformations of inorganic species into ashes and deposits under reducing atmospheres. The following areas of research will be emphasized over the remainder of the project:

- The study of deposition and strength development mechanisms using the PDTF
- The continued evaluation of the physical properties affecting ashes and deposits which result in high-strength deposits

ACKNOWLEDGMENTS

The Energy & Environmental Research Center would like to thank the sponsors of this project for their desire to continue developing the future of the Fossil Energy Program. The six sponsors are Shell Oil Company, Texaco, DOW Chemical Company, Netherlands Energy Research Foundation the Electric Power Research Institute, and the U.S. Department of Energy.

REFERENCES

Erickson, T.A.; Brekke, D.W.; Folkedahl, B.C.; Tibbetts, J.E.; Nowok, J.W.; Benson, S.A. "Coal Ash Behavior in Reducing Environments," Presented at the Coal-Fired Power Systems 93 — Advances in IGCC and PFBC Contractors' Review Meeting, Morgantown, WV, June 28-30, 1993.

Kalmanovitch, D.P.; Frank, M. "An Effective Model of Viscosity for Ash Deposition Phenomena," Conference on Mineral Matter and Ash Deposition from Coal; The Engineering Foundation, Santa Barbara, CA, February 21-26, 1988.

Steadman, E.N.; Zygarlicke, C.J.; Benson, S.A.; Jones, M.J. "A Microanalytical Approach to the Characterization of Coal, Ash, and Deposits," In Seminar on Fireside Fouling Problems, ASME Research Communication on Corrosion and Deposits from Combustion Gases, Washington D.C., 1990.

Urbain, G.; Cambier, F.; Deletter, M.; Anseau, M.R. *Transitions of the Journal of the German Ceramic Society* **1981**, *80*, 139.

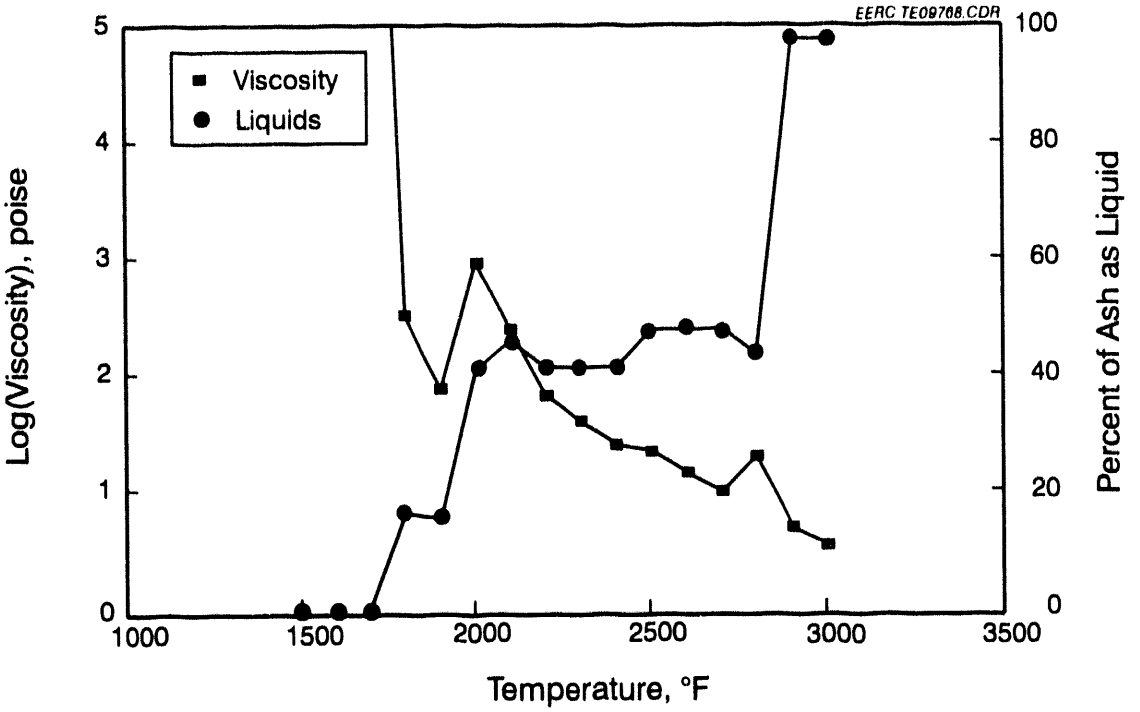

Figure 3. Thermochemical Equilibrium Modeling of a Slag Formed from the Gasification of Coal A

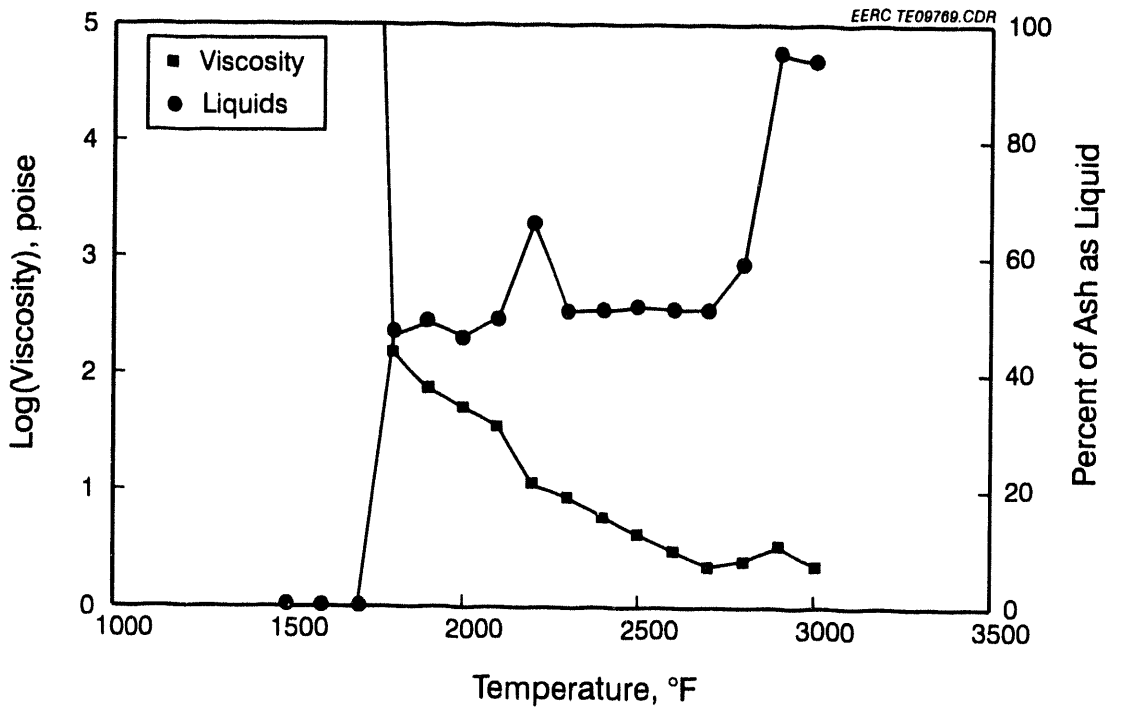

Figure 4. Thermochemical Equilibrium Modeling of a Slag Formed from the Gasification of Coal B

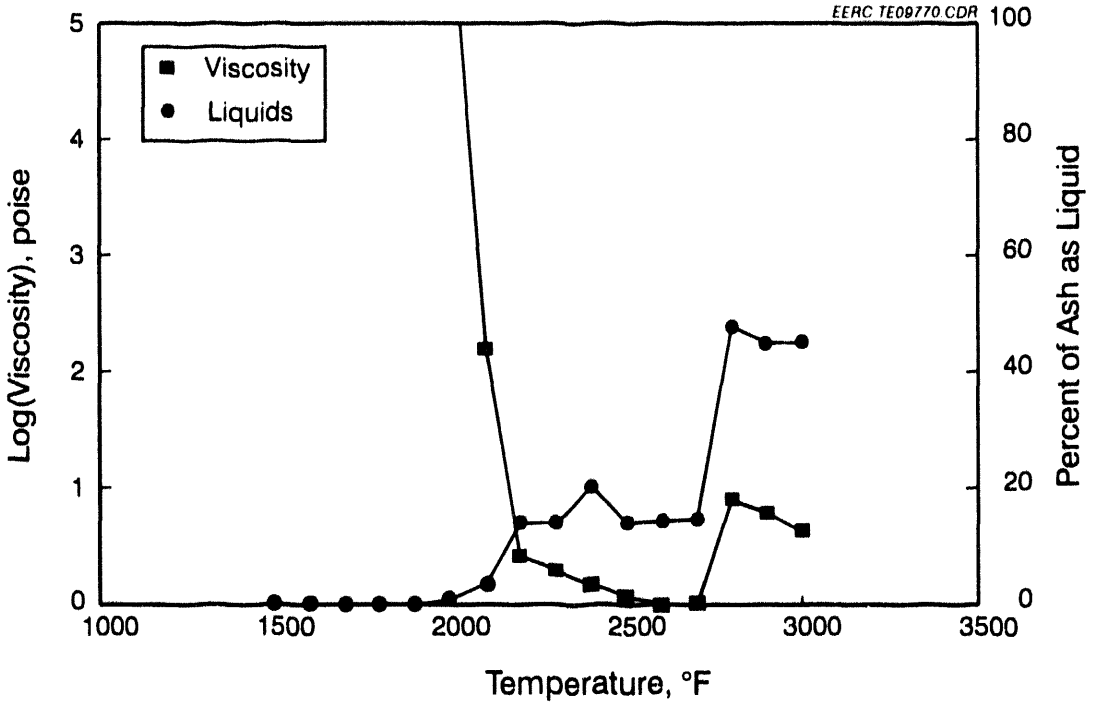

Figure 5. Thermochemical Equilibrium Modeling of a Slag Formed from the Gasification of Coal C

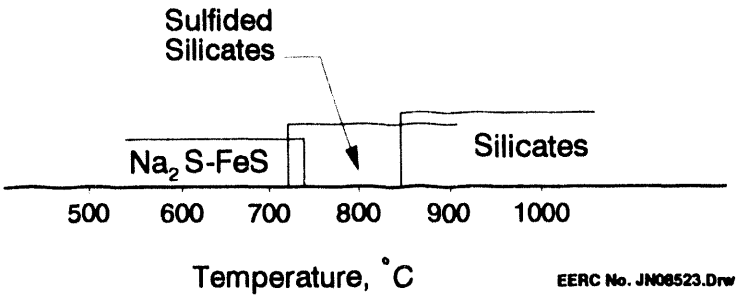

Figure 6. Diagram Showing a Sintering Model of Coal Ashes in Three Different Ranges of Temperatures and in the Presence of Three Possible Liquid Phases

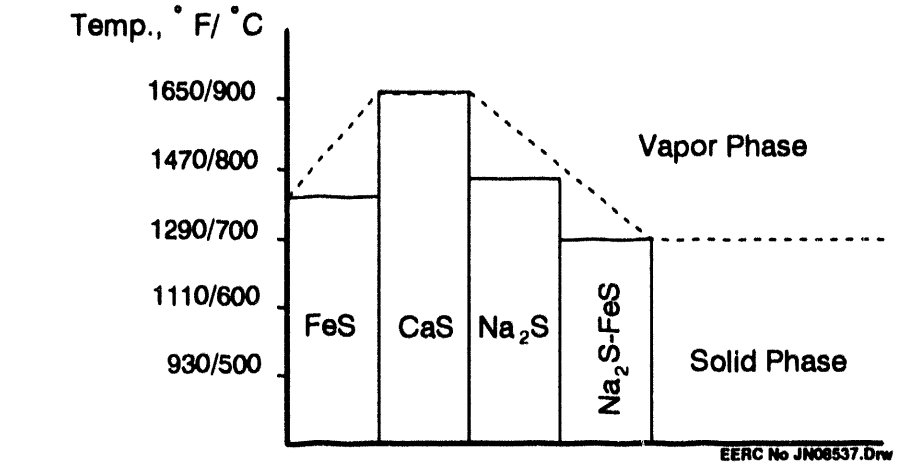

Figure 7. Thermal Stability of Major Sulfides Derived from Coal Ashes under Gasification Conditions

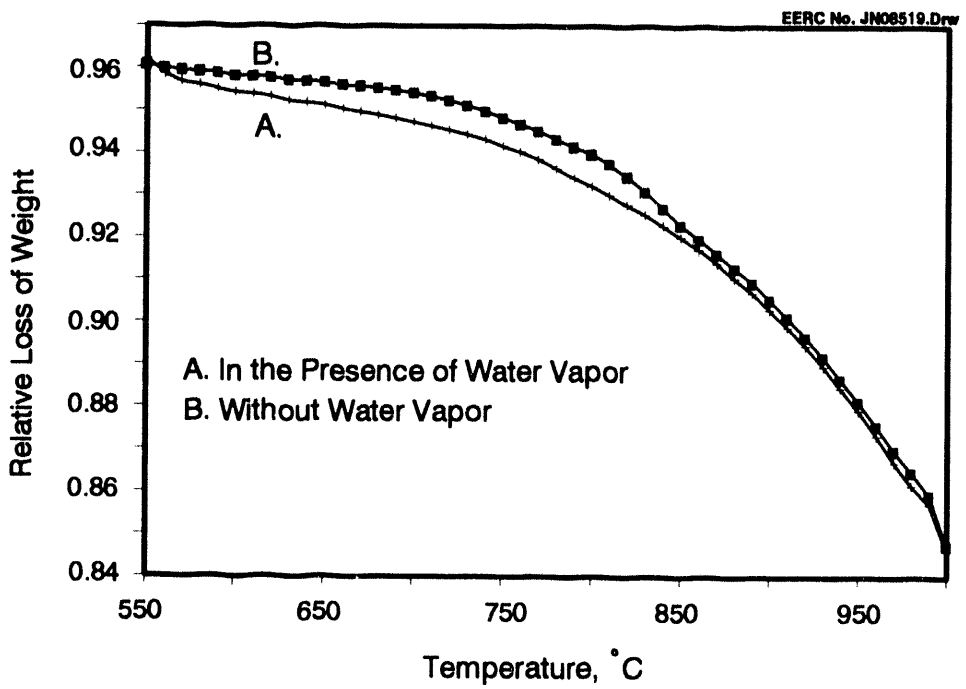

Figure 8. The Relative Loss of Weight of $Fe_{1-x}S$ in the Presence and Absence of Water Gas under Reducing Conditions

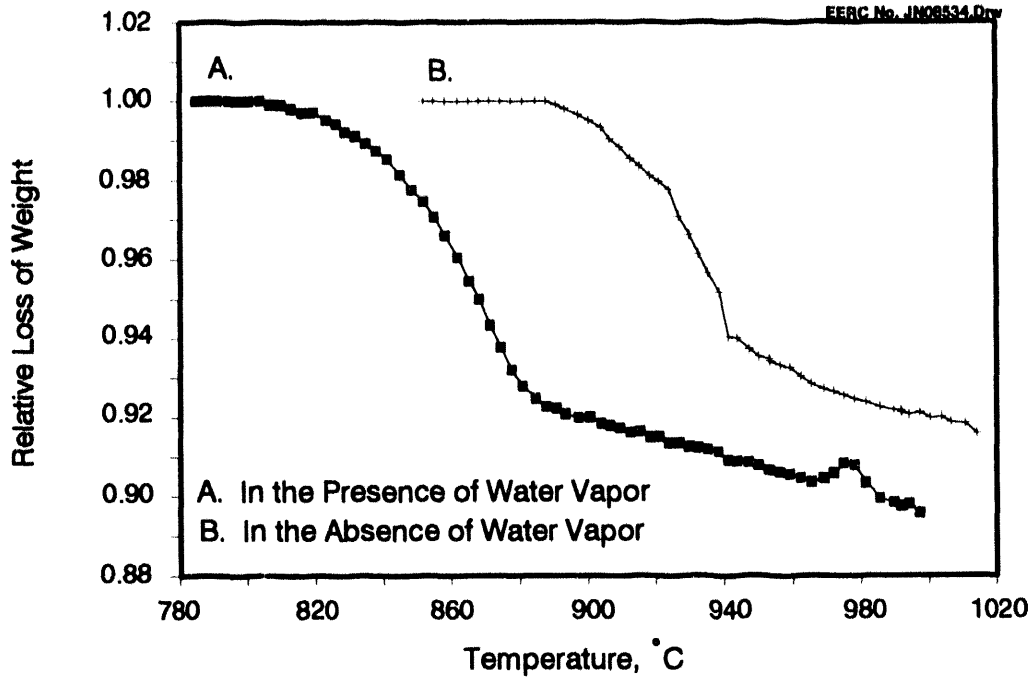

Figure 9. The Relative Loss of Weight of CaS in the Presence and Absence of Water Gas under Reducing Conditions

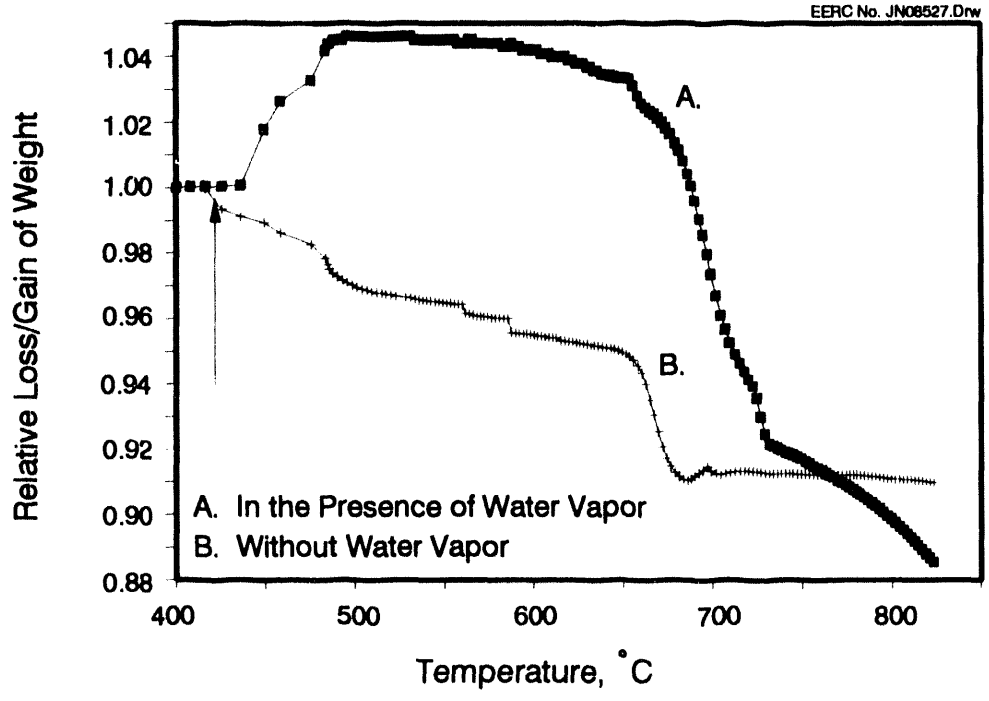

Figure 10. The Relative Loss of Weight of Na_2S-1.7 FeS in the Presence and Absence of Water Gas under Reducing Conditions